LUND UNIVERSITY

EXPERIMENTAL TESTING OF BIRCH WOOD

Fracture energy and its applicability in dowel-type joints

EMMA ESBJÖRNSSON and JOHAN SVENSSON

Structural Mechanics

Master's Dissertation

DEPARTMENT OF CONSTRUCTION SCIENCES

DIVISION OF STRUCTURAL MECHANICS

ISRN LUTVDG/TVSM--24/5275--SE (1-78) | ISSN 0281-6679

MASTER'S DISSERTATION

EXPERIMENTAL TESTING OF BIRCH WOOD

Fracture energy and its applicability in dowel-type joints

EMMA ESBJÖRNSSON and JOHAN SVENSSON

Supervisor: **HENRIK DANIELSSON**, Associate Professor, Division of Structural Mechanics, LTH.
Assistant Supervisor: **JOHANNES JONASSON**, MSc, Division of Structural Mechanics, LTH.
Examiner: Professor **ERIK SERRANO** Division of Structural Mechanics, LTH.

Printed by V-husets tryckeri LTH, Lund, Sweden, June 2024 *(P1)*.

For information, address:
Division of Structural Mechanics,
Faculty of Engineering LTH, Lund University, Box 118, SE-221 00 Lund, Sweden.
Homepage: www.byggmek.lth.se

Abstract

In this study the fracture energy has been evaluated for birch, which is a relatively common hardwood in Sweden. The Nordtest method has been used to extract the fracture energy through a 3-point bending setup. The fracture energy was studied in the weakest load orientation of the orthotropic wood, which was tensile loading perpendicular to its grain. The directional systems of radial-longitudinal (RL) and tangential-longitudinal (TL) were implemented and tested. The RL direction showcased a higher fracture energy than the TL direction, but it did at the same time display more unstable results. Two different shapes of fracture areas of the Nordtest specimens were tested, the rectangular shape as described in the standard, and a triangular shape. The unstable results were mainly from RL loading with a rectangular fracture area. The specimens with a higher density showcased both tendencies for a higher load capacity and a higher fracture energy.

The experimentally obtained fracture energy was then implemented to calculate the splitting capacity of dowel-type joints, which were made from the same boards used for manufacturing the Nordtest specimens. The dowel joints were then created, tested and examined. The calculated and experimental data were then compared. The calculated capacity was higher than the experimental capacity, maybe due to an unknown/assumed shear modulus. Beams with a higher density and a prescribed minimum dowel edge distance (from Eurocode 5) also showcased a higher load carrying capacity. Beams with a shorter dowel-to-edge did not showcase a higher load capacity in relation to a higher density. The beams with a longer edge distance had a higher capacity, due to premature splitting being avoided, which was indicated by a larger dowel hole deformation. The beams with a smaller edge distance tended to have a smaller embedment deformation and a lower capacity.

Sammanfattning

I denna studie har brottenergi utvärderats för björk som är ett av de vanligaste lövträden i Sverige. Nordtest-metoden användes för att bestämma brottenergin genom trepunkts böjning. Brottenergin studerades i den svagaste belastningsorienteringen hos det ortotropa träet, vilket var dragbelastning vinkelrätt mot dess fibrer. Provningarna gjordes med en radiell-longitudinell (RL) och tangentiell-longitudinell (TL) sprickorientering. RL-riktningen visade en högre brottenergi än TL-riktningen men uppvisade samtidigt fler instabila resultat. Två olika former på brottytan för Nordtest-provkropparna testades, en rektangulär form som beskrivs i Nordtest och en triangulär form. De instabila resultaten uppkom främst hos provkroppar med en rektangulär brottarea och som belastades i RL-riktningen. Provkropparna med högre densitet uppvisade tendenser till en högre bärförmåga och en högre brottenergi.

Den experimentellt erhållna brottenergin implementerades sedan för att beräkna uppsprickningskapaciteten för ett dymlingsförband, som tillverkades av samma planka som provkropparna i Nordtest-metoden. Dymlingsförbanden skapades, testades och undersöktes. Den beräknade och experimentella kapaciteten jämfördes därefter. Den beräknade kapaciteten var högre än den experimentella, möjligen på grund av en okänd/antagen skjuvmodul. Provkropparna med högre densitet och ett föreskrivet minimalt avstånd till kanten för dymlingen (enligt Eurokod 5) uppvisade också en högre bärförmåga. Balkar med kortare avstånd från dymling till kant visade inte en högre bärförmåga i förhållande till en högre densitet. Provkropparna med ett större kantavstånd hade en högre kapacitet eftersom tidig uppsprickning undveks, vilket indikerades av en större deformation av dymlingshålet. Provkropparna med ett mindre kantavstånd tenderade att ha mindre hålkantsdeformation och en lägre kapacitet.

Acknowledgements

This dissertation was conducted during the spring 2024 at the Division of Structural Mechanics in fulfillment of the requirements for the degree of Master of Science in Civil Engineering at Lund University.

We would like to thank our examiner Erik Serrano and our supervisor Henrik Danielsson, for always being available for discussing ideas and helping us with progressing in the work. Thank you, Johannes Jonasson for giving us valid inputs regarding the experimental setup. We would also like to thank Jessica Dahlström, Stefan Backe and Martin Gunder for helping us with the experimental testing and in the wood workshop.

The birch material used for experimental testing within this project was provided by Research Institutes of Sweden (RISE), via Edinburgh Napier University in Scotland. We thank Ulf Lemke and Marlene Cramer for the support in this process.

Lund, June 2024
Emma Esbjörnsson & Johan Svensson

Notations and Symbols

Latin letters

L	Longitudinal direction
R	Radial direction
T	Tangential direction
l	Length [m]
r	Radius [length unit]
w	Deformation [m]
U_c	Elastic energy [J/m]
E	Young's modulus (modulus of elasticity] [Pa]
G_f	Fracture energy [J/m^2]
G_c	Critical energy release rate [J/m^2]

F	Reaction force [N]
h	Height [m]
h_e	Dowel- to edge distance [m]
t	Thickness [m]
d	Diameter of dowel [m]
f_h	Embedment strength [Pa]
M_y	Yield moment [Nm]
k_{90}	Scaling factor
f_u	Tensile strength [Pa]

M	Bending capacity [Nm]
f_m	Strength parameter [Pa]
W	Section modulus [m^3]
k_{crit}	Factor accounting for effect of lateral buckling
G	Shear modulus (modulus of rigidity) [Pa]
I	Moment of inertia [m^4]

a	Height of cube [m]
b	Length of cube [m]
c	Width of sawn notch [m]
h_{cut}	Height of fracture area [m]
W	Work [Nm]
m	Mass [kg]
g	Gravitational acceleration [m/s^2]
A	Area [m^2]
u	Moisture content [%]

Greek letters

σ	Stress [Pa]
ϵ	Strain [%]
ρ	Density [kg/m^3]
α	Angle between load and fibre direction [deg]
λ	Slenderness ratio

Contents

1 Introduction

This chapter is an introduction to this study, describing the background to why investigating the fracture energy of birch is a subject of interest. The aim of the study is presented as well as an overview of the method used to achieve the goals of this study. Some limitations are also introduced to narrow the scope of the experiments.

1.1 Background

Wood is a renewable resource and it has always been a popular construction material. Today, approximately 90% of all single-family houses in Sweden have a supporting frame made of wood. The usage of wood in multi storey buildings is not as high, approximately 20% in Sweden, but it is rising [1]. The advantages of using wood as a construction material is the combination of low dead weight and high insulating abilities. The disadvantages are its low resistance against moisture which may lead to rot and decomposition.

The Swedish forests consists of 83% coniferous forests, i.e a forest primarily occupied by evergreen plants that have needle-leaves, such as pine and spruce. Around 5% of the forest in Sweden is deciduous forest, plants that loses their leaves annually (for instance birch). The reaming 12% of the forests in Sweden are a mix between coniferous and deciduous plants. The distribution between different species of wood is shown in figure 1.1, where birch is the most frequent deciduous plant [2]. According to Skogskunskap (2024) [3], birch constitutes 2/3 of the deciduous forest in Sweden and there are mainly two species of birch, silver birch (*Betula pendula*) and downy birch (*Betula pubescens*). The former exist with a higher frequency in the southern part of Sweden, whereas the latter, Betula pubescens, has a presence in the northern part of Sweden.

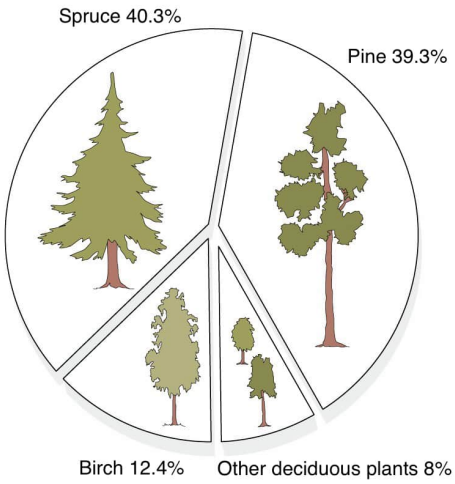

Figure 1.1: The standing forest stock in Sweden distributed by species in percentage, modified after [2].

A forest consisting of a higher amount of deciduous plants has a lower risk of fast spreading forest fires thanks to the water stored in the leaves. It also contributes to a higher biodiversity. Since the proportion of birch is predicted to rise, it is of interest to increase the knowledge in the material properties of birch. Moreover, it is also of interest to evaluate if birch is a competitive construction material compared to spruce and pine [4].

Birch has equivalent characteristics as spruce and pine when it comes to the technical properties and quality classification, according to Ödlund [5]. Ödlund means that the disadvantages of using birch in comparison to spruce and pine is the ability to resist moisture. If the construction is protected from water and moisture, birch could be a competitive material when it comes to using it as a construction material.

Today, most of the Swedish birch is used as firewood or in pulp mills [5]. Approximately one percent is used for furniture and joinery. One reason for this, birch not being used as a construction material, is that there is no strength grading or CE-marking standard for birch that has grown in Sweden [6]. Since there is no standard, there is a low interest in building sawmills that are focused on sawing birch. This leads to a lower demand and a higher prices.

To use birch for structural applications, numerous material properties need to be known. These properties are implemented in various calculation models. In this study, the material property called fracture energy, which is the energy required to create a unit area of crack surface, will be investigated. There are multiple ways to obtain the fracture energy, but in this study the Nordtest method, NT Build 422 [7], will be used. Earlier studies by Lai and Plönning [8] show an uncertainty regarding the Nordtest method as the experiments produced invalid results for birch. Therefore, it is relevant to examine different alterations of the test setup and specimen geometry to determine if the method is applicable for birch.

The birch in this study was provided from a project, BizWOOD run by RISE [6], where the objective is to develop strength grade rules for Swedish birch. The exact location from where the birch in this study was grown is unknown, but they originate from the same area in Sweden. The species used in this project are either Betula Pendula or Betula Pubescens, but it is unknown which species was tested. The reason for this is that the material was delivered from the sawmills unmarked. Once cut down into pieces, it is not possible to distinguish the two species apart by visual inspection. Therefore, both species of birch are further mentioned as birch.

1.2 Aim

Earlier studies regarding the fracture energy in wood have been conducted on a limited scale. The aim of this project is to further expand the knowledge and the database concerning the fracture energy for birch produced in Sweden.

The Nordtest method, used for testing the fracture energy, has been proven inefficient for some wood species. In this study, a different notch geometry for the specimens is tested and it is discussed whether the method should be reevaluated.

The application of Eurocode 5 is limited regarding the splitting capacity of hardwood. In this study, a comparison between the actual and the calculated capacity for birch is evaluated. The actual capacity is measured by conducting experiments using a dowel-type connection, where the wood is subjected to a force perpendicular to the grain. The design formula of Eurocode 5, which is based on fracture mechanics theory, is used as comparison to the experiments.

1.3 Method

A literature study about the mechanical properties and material structure of wood was performed. Also a study about fracture mechanics, with focus on linear and nonlinear fracture mechanics, and different crack orientations was of interest. The study was done in order to determine whether the Nordtest method was suitable for examining the fracture energy in the material.

In order to obtain the fracture energy from the birch, experimental tests had to be carried out. The tests were conducted in accordance with the Nordtest method, which is a method for determining the fracture energy in wood at tension perpendicular to the grain through 3-point bending.

The obtained fracture energy's applicability was then tested for a dowel-type connection with load perpendicular to the grain. These tests were done in accordance with the Eurocode 5's suggested calculations for dowel-type joints. Several beams made of birch, were cut out and tested. The experimental and calculated results were then compared.

Results from both the Nordtest method and the dowel-type joint tests were compared to other available literature.

1.4 Limitations

The work presented in this study is restricted by the following limitations:

- The material provided to this study is birch, but the specific species is unknown.
- The tests in this study were performed on four individual boards from the same sawmill. Their geographical origin in Sweden is unknown.
- Only short term loading is considered.
- The crack orientation of the test specimens is assumed to be either pure RL or TL direction.
- Clear wood is used when the fracture energy of the wood material is determined i.e the material has no knots or other defects. The results in this study is therefore not representative for structural-sized timber. Further studies and test must be performed.
- The deformation occurring in the wood at the supports, when the dowel-type joints are tested, is disregarded.

2 Properties of wood

To be able to understand how the mechanical behavior of timber varies with regard to which direction a load is applied, it is of importance to study the structure of the timber. In this study, only a general overview regarding the macro and micro structure will be presented. The mechanical properties of wood, such as strength, toughness and stiffness depend mainly on three things: density, moisture content and the angle of the fibre in the wood [9].

2.1 Material structure

Trees have developed over millions of years and therefore it is easy to understand that the qualities and structures of the tree are well adapted for its purpose. The purpose of the stem of the tree is to withstand the horizontal wind forces, the vertical dead weight of the tree itself and to transport nutrients and water to the top of the tree [10]. Trees are adapted to provide the maximum strength in their longitudinal direction, compression parallel to the fibers. In addition, it has a high bending stiffness against horizontal loads. Forces perpendicular to the fibers are not naturally occurring to trees and therefore the wood is not as strong in this direction in comparison.

Wood is a natural material, affected by nature, meaning there will be defects in the wood such as knots and splits. Larger test subjects are more likely to contain more defects compared to a smaller subject. Defects like these tend to create cracks in the wood, redistributing stresses in the material [11]. A smaller test body would be stronger with the absence of said defects [11]. In material testing, where ideally perfect test specimens are used, a representative value for larger construction contexts is therefore not always obtained. Wood without defects and knots is referred to as clear wood [12].

2.1.1 Hardwood and softwood

Wood can be divided into two categories, hardwood and softwood, and they are botanically quite different. Softwoods often come from conifers, trees with needle-like leaves, more commonly known as evergreen trees. Conifers do not shred their leaves annually and remain green all year. Hardwoods, also known as deciduous trees, are trees with broad leaves which they shred every year. These are some of the differences in external appearance, but they also differ from each other internally, structurally and morphologically [13].

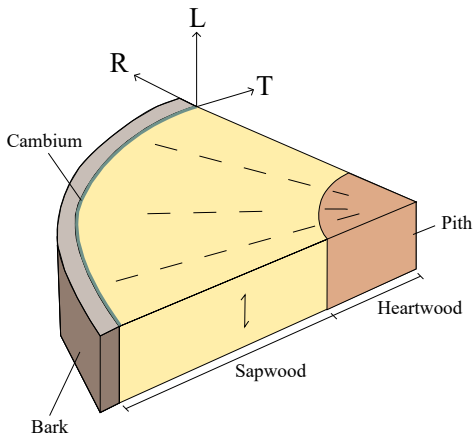

Figure 2.1: Orientations and parts of a wooden stem, inspired from [8].

2.1.2 Orthotropy of wood

The structure of the tree gives the wood its orthotropic characteristics, properties that are different along three perpendicular axes orientated in the stem. Since the characteristics of the wood depend on which direction the wood is loaded, it is of importance to understand how the load is applied. The three principal axes, shown in figure 2.1, are called the longitudinal (L), the radial (R) and the tangential (T) directions. The longitudinal axis is parallel to the fiber of the wood, the radial axis is normal to the growth rings and perpendicular to the directions of the fiber. The tangential axis is also perpendicular to the fiber direction but it is a tangent to the growth rings i.e perpendicular to the radial axis.

2.1.3 Macro structure

The macro structure of the wood includes the parts in the stem that are visible to the eye. In the transversal direction, the trunk can be divided into different concentric layers: bark, cambium, sapwood and heartwood. These layers are shown in figure 2.1. The outer layer, the bark, is divided into the outer and inner bark. The outer bark protects the tree from water loss and parasites and the inner bark transports nutrients from the leaves down through the stem to the cambium and the roots. The cambium is a thin layer located inside of the bark. Tree growth occurs in the cambium layer. Outwardly the cambium produces bark and inwardly, wood cells are produced [1, 10] . The wood cells produced in the cambium form the sapwood. In this layer, a liquid known as sap, containing water and dissolved nutrients, is transported from the roots of the tree. Heartwood is the layer inside of the sapwood, seen in figure 2.1. The two layers consist of the same cell type but in the heartwood the cells start to produce substances called resin, which hinder water transportation. The resin in the heartwood contributes to the overall stability of the trunk and the extractive shields the tree naturally from water reliant organisms. The heartwood is normally darker than the sapwood, but not for every species. The pith, which is located in the middle of the stem, serves as a way of transporting nutrients and water in the tree. To enable transportation between the pith and the bark there are also horizontal cells called rays. [1, 10]

During the year, the tree develops different kinds of cells in the sapwood. In the spring, the trees are in a great need of cells that can transport water and nutrients, therefore the cells formed have thin cell walls and large cavities [1, 10] . This kind of cells are called earlywood. During the summer and autumn, the need for transportation of water is much lower and the need for stability to withstand wind, and later snow, becomes more prominent. The cells that are produced during this time of the year are called latewood and they have a thicker cell wall and smaller cavities than the earlywood. The part in the stem that consists of earlywood is often broader and lighter in color than the latewood layer, that often is thinner and darker. Every year, one layer of earlywood and one layer of latewood is produced in the tree, which combined form an annual growth ring. The thickness of the different layers depend on the temperature and climate conditions during which the layers were formed. Therefore, the widths of the growth ring could vary from year to year. [1, 10]

The wood closest to the pith, the first 5-20 growth rings, is called juvenile wood [10]. The juvinele wood is formed during the first years of the trees growth. During this time period, the growth of latewood is not as prevalent as the growth of the earlywood. As a result, the density and strength is lower in this part of the wood than in the later formed part of the stem, also known as mature wood.

2.1.4 Micro structure

Looking at a tree in a macroscopic scale, hardwoods and softwoods are quite similar. When studying them in a microscopic scale they differentiate quite a lot. Hardwoods have a much more complex structure, consisting of many different cell types, contrary to the softwoods which have a relatively simple structure, consisting of only a few cell types [13].

The wood consists of cells oriented in both the longitudinal and radial direction. In softwoods, approximately 90-95% of the total volume is composed of longitudinal tracheids. This cell type is also found in hardwoods, but in a much smaller proportion. For hardwoods, the longitudinal tracheids are approximately 75% shorter than in softwoods. Apart from trecheids, hardwood contains multiple types of longitudinal cells, e.g. vessels and fibers. These are specialised in either transporting nutrients or working as a structural support in the wood. Thanks to the specialised cells, and a more complex structure, hardwood is often stronger than the softwood according to Shmulsky [13].

Accordning to Shmulsky [13] the amount of ray cells, cells that transport nutrients in the horizontal direction in the stem, only constitutes about 5-7% of the volume in softwoods. In hardwoods the average volume of ray cells are 17% of the total volume, often adding to the overall strength.

2.2 Moisture and wood

The moisture content, which varies with the relative humidity, is almost identical between different wood species at the same relative humidity [9]. This is explained by the fact that they are made from the same compounds: lignin, hemicellulose and cellulose.

According to Forsman [12], the stiffness, strength and fracture energy of the wood is affected by moisture content. The strength and stiffness of the wood tends to be the highest at around 0-75% relative humidity, decreasing thereafter as the wood softens. More importantly, the fracture energy is moisture dependent [12].

3 Fracture mechanics

This chapter presents the basics of fracture mechanics (and how it is applied).

3.1 Crack orientations

The characteristics of the fracture in wood depend on how the material is loaded, which mode of loading the material is subjected to and the orientation of the crack plane. There are three different types of modes of fracture. The different modes are shown in figure 3.1 where mode I represents cracking due to tensile stress perpendicular to the crack plane, also known as the opening mode [14]. Mode II occurs when the material is subjected to shear stress acting parallel to the crack plane and in the crack propagation direction. Mode III is when the material is subjected to a shear stress parallel to the crack plane and perpendicular to the crack propagation direction. In practical applications, e.g. in structural elements, the material is loaded with a combination of the three different modes, also known as mixed mode loading or mixed mode fracture. The most common one is the combination of mode I and II, which occurs around holes in beams or in dowel-type connections loaded perpendicular to the grain [14].

Due to the orthotropic properties of wood, there are six possible principal crack plane orientations and propagation systems. The crack plane orientations are based on the longitudinal (L), radial (R) and transversal (T) orientations shown in figure 2.1, which depicts the cross section of the stem of a tree.

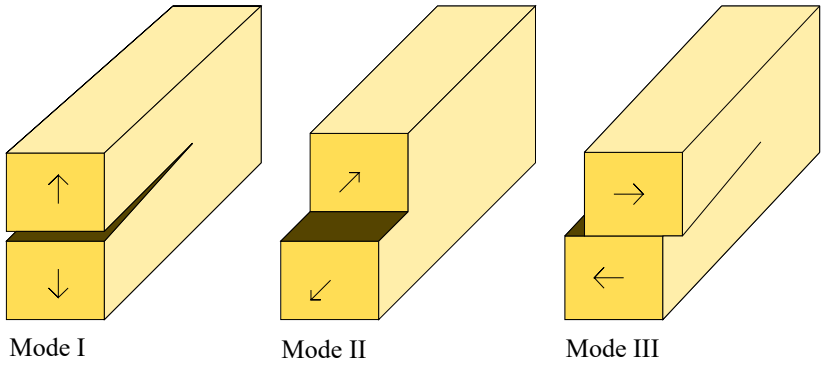

Figure 3.1: Different modes of fracture for wood, inspired from [15].

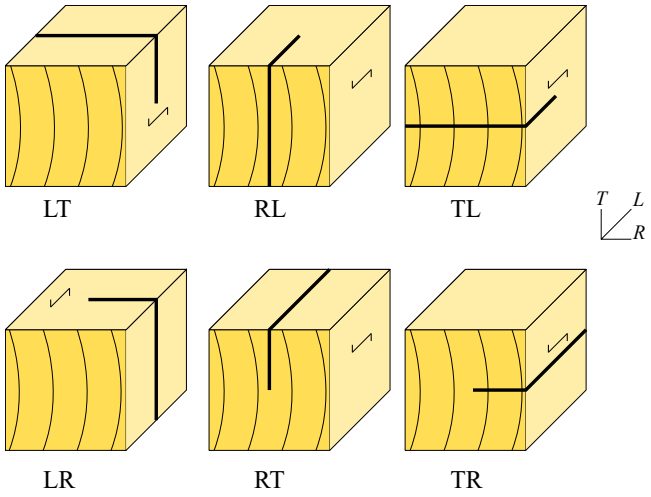

Figure 3.2: Possible orientations of crack planes in wood, inspired from [15].

Figure 3.2 show the six possible principal crack plane orientations and propagation systems. The fist letter indicates the normal of the fracture surface and the second letter denotes the direction in which the crack propagates. The RL, TL, RT and TR directions, the directions exposed to tension perpendicular to the grain (crack propagation along the grain), are the most common ones to test since these are the directions that are the most relevant for practical applications [14]. Also, wood is the weakest in these directions. This study will thereby investigate the RL and TL crack plane orientations and propagation systems.

3.2 Stress distributions and relations

According to Wadsö [11], the fracture mechanics for tensile loading can be understood by analyzing different areas of a loaded material. It is of interest to study the material's response prior- and after the material capacity is reached.

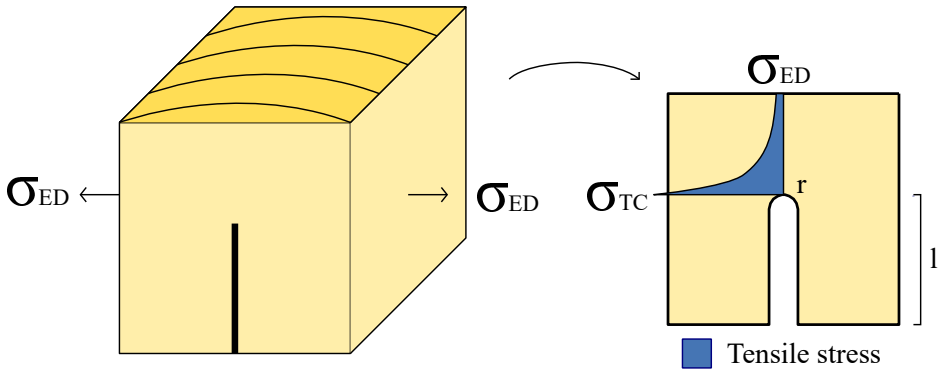

Figure 3.3: Tensile stress distribution at the tip of a crack, induced by an evenly distributed tensile stress. Re-constructed from [11].

As a crack first appears, the stress concentrates at the tip of the crack [11], as seen in figure 3.3. The assumption of the material behaving linearly yields 3.1 for the stress at the tip of the crack, σ_{TC}.

$$\sigma_{TC} = \sigma_{ED}(1 + \sqrt{\frac{l}{2r}}) \tag{3.1}$$

Where σ_{ED} is the distributed stress, l is the crack length and r is the radius of the crack's tip. The crack having a smaller radius, resulting in a thinner crack, yields increasingly higher stresses, approaching infinity as the radius approaches zero [11]. However, real materials do not have ideal elastic properties nor do they withstand infinitely large stresses and strains. The materials will instead plasticise and/or crack before the infinitely large stresses occur [11]. This results in the high stresses being redistributed over an area called the fracture process zone (FPZ). This redistribution decreases the stress concentration at the tip of the crack, a phenomenon which can be described based on concepts according to non-linear fracture mechanics [15].

3.3 Fracture energy relations

Testing of the fracture energy for wood, among other materials, can be done by subjecting the material to a tensile load with a constant deformation rate until the material ruptures [11]. With the constantly applied displacement, a stress-strain (σ-ϵ) and stress-deformation (σ-w) relation can be obtained. The first linear (and potentially non-linear) stress-strain relation describes the material prior to reaching maximum stress capacity. The stress-displacement relation describes the material after reaching its maximum stress capacity [11, 15] . Combined, both relations form a complete description of the rupturing material's fracture energy, from initiated fracture until the material eventually breaks, the complete failure [11].

The stress-strain and stress-deformation relations for a body in tension can be summarized in figure 3.4, where the strains and deformation have been separated. The strain and body length relation, $\epsilon \cdot l$, represents the elastic energy stored in the material and the deformation graph shows the fracture energy in the FPZ [15].

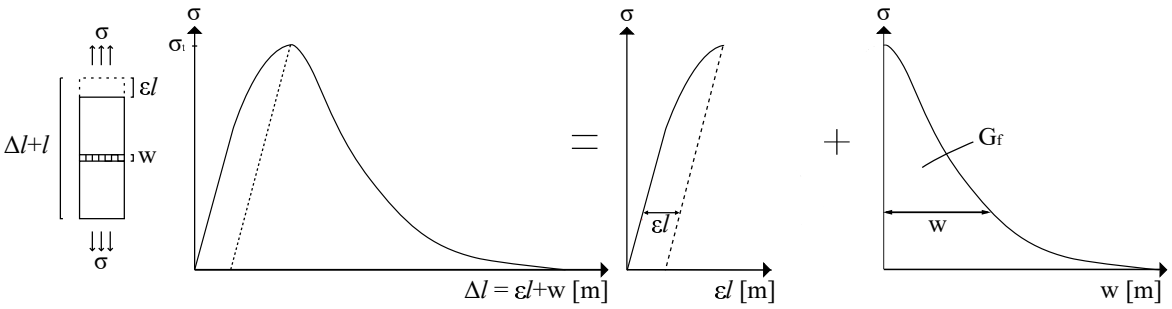

Figure 3.4: Complete overview of strain and deformation relations to body tensile strain. Re-drawn from [15].

As a material is subjected to a uniform tensile stress, it deforms evenly throughout the body. But as a FPZ develops, all deformation will continue to concentrate in the FPZ whereas the rest of the body linearly deforms back to its original state. The nature of the eventual rupture, which is either brittle or ductile, depends on the amount of elastic energy, U_c, that is stored in the body and the body's length. The elastic energy is the energy released when the body retracts after material rupture [11]. The elastic energy is obtained during the elastic deformation phase and it can be described with the elastic modulus, E, and the tensile strength, σ_t, as:

$$U_c = \frac{\sigma_t^2}{2E} \tag{3.2}$$

The area under the σ-w curve, in figure 3.4, for the entire body describes the fracture energy G_f [15], with the stress being a function of the displacement, w:

$$G_f = \int_w \sigma(w)dw \tag{3.3}$$

The fracture energy is also defined as the amount of energy needed to grow a crack one unit area.

The fracture is either ductile or brittle and the length of the specimen is vital to determine the outcome, creating the following criteria for a brittle failure:

$$U_c l > G_f \tag{3.4}$$

The formula suggests that a longer specimen stands a larger risk of brittle failure, as the length is multiplied with the elastic energy stored in the material. The specimen length which yields brittle failure is called the critical length [11].

3.3.1 Determining the fracture energy

One way to obtain the fracture energy is by subjecting a bar element, of the arbitrary material, to pure tensile forces and measuring the force-deformation response [11].

Reaching the sought tensile stresses perpendicular to the grain could be done in numerous ways, one of them being 3-point bending. A method for conducting this experiment is described in chapter 5 which explains the Nordtest method. The Nordtest method is depicted in figure 3.5 and it achieves tensile stresses just above the cut in the cube specimen. As stated in the report by Lai and Plönning [8] the specimen being subjected to 3-point bending yields varying stress-levels, both compressive and tensile, along the cross-section as the test body is displaced.

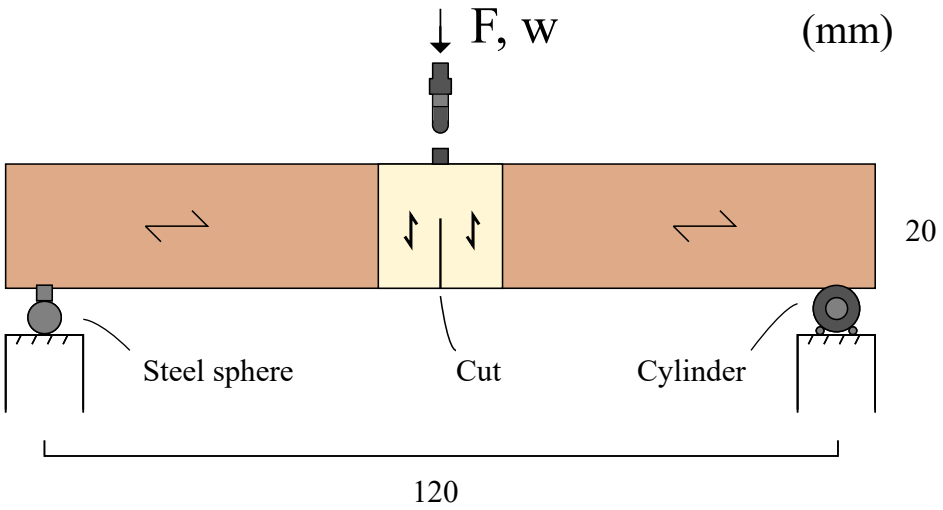

Figure 3.5: The 3-point bending test setup inspired by the Nordtest method [7].

Looking at figure 3.6 and 3.7, the modeling from Lai and Plönning [8] suggests that the following (roughly illustrated) stress distribution could be seen at point a-d of the force-displacement relation. In a), the lower part is subjected to large stresses as the damage zone begins to develop. In b) and c), the material has started to behave in a non-linear manner. Here, stresses on the bottom edge diminish as the material softens and a fracture process zone is formed [15]. In c), which is the point just before the maximum bending capacity is reached, the lower edge is under less stress than in b) which indicates that a crack will appear. Right after c) the material ruptures and the next non-linear phase d) begins. This is where the crack is developing from the lower edge. The compressive and tensile stress distribution then moves up the cross-section to maintain equilibrium as the crack progresses [8].

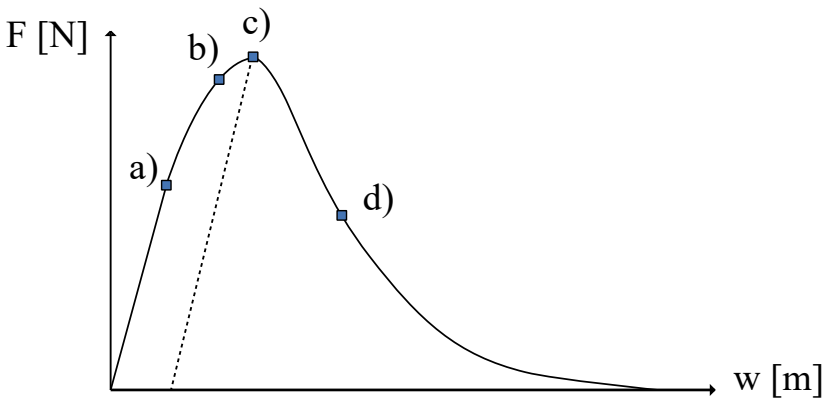

Figure 3.6: Stages for each cross section stress. The figure shows the measured force in relation to displacement, inspired from [8].

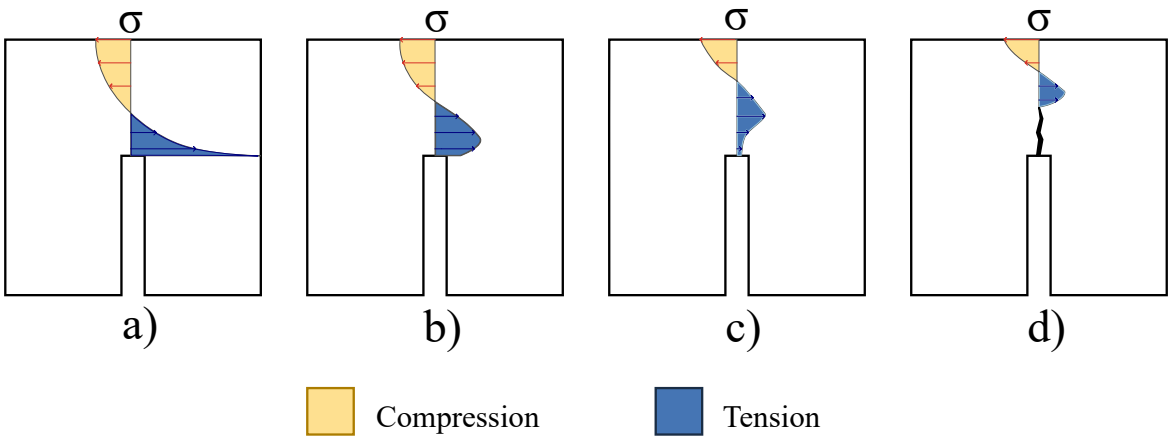

Figure 3.7: Stress distribution through cross section, inspired from [8].

In figure 3.8, an evenly distributed tensile force is applied on an imagined bar element with the length L_c. The 3-point bending is a way of achieving a bar element in tension, making it possible to measure the fracture energy according to the method explained by Wadsö [11]. To be able to utilize this theory, the shape of the cut in the specimen should not be similar to the one showed in figure 3.3, where a rounded tip is showed. The shape of the cut would, according to Nordetest [7] and Lai and Plönning [8], affect where the stresses concentrates. However, this phenomenon was not considered for further experimental testing since no method of verifying the shape of the cut was used. The cut in every sample was assumed to be identical since same blade was used each time.

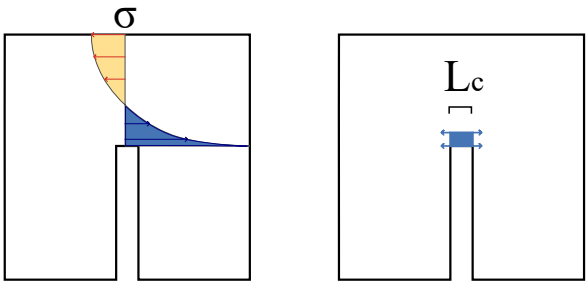

Figure 3.8: The cross section of the test cubes with a high tensile stress at the edge of the notch. The stress is applied on an imagined bar element with length L_c.

4 Joints and Eurocode

Dowel-type joints are implemented in almost every wooden structure with varying complexity. The connection can be between two wooden components or wood and steel plates. For every connection, the wood, dowel and steel plate should have known parameters, such as geometry and structural properties. The amount of shear planes between wood and steel is also needed to be known.

The Nordtest method tests the fracture energy during loading perpendicular to the grain. A way of implementing and verifying the fracture energy perpendicular to the grain is to construct a suitable dowel joint. The constructed dowel-joint used in this study is shown in figure 4.1. A loading angle of 90 degrees perpendicular to the fibre direction is implemented. The aim of the dowel tests was to evaluate and verify the obtained fracture energy from the Nordtest method.

The dimension of the dowel, wooden beam and steel plates (located on each side of the beam) was chosen carefully so that the right failure of the joint would occur. Three different types of failure modes could occur in this type of setup, where a beam is subjected to a point load perpendicular to the grain in the center of the beam. There could be an embedment failure, a bending failure or failure due to splitting. In the following sections these three different types of failure modes will be discussed. The goal was to reach a fracture where the wood breaks without the dowel or plates experiencing plastic straining. Furthermore, deformation in the wood around the embedded dowel (embedment failure) is not desired.

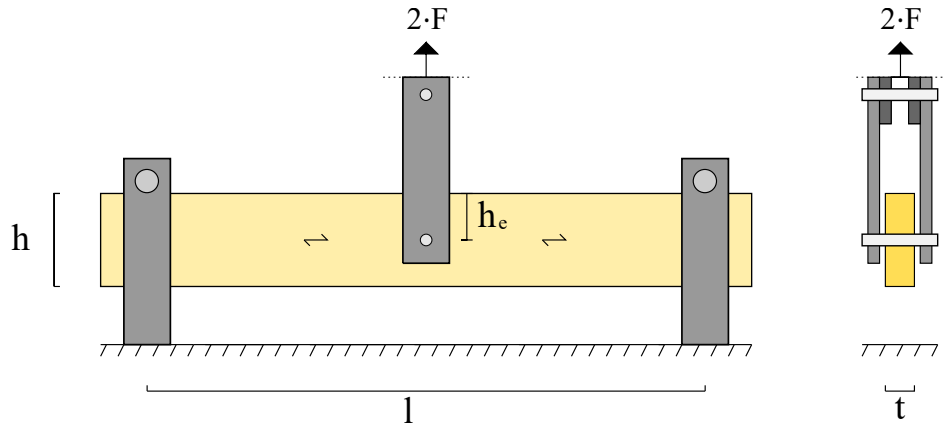

Figure 4.1: Beam setup for failure mode testing. The minimum distance h_e is the distance from the edge to the centre of the dowel, inspired from [12].

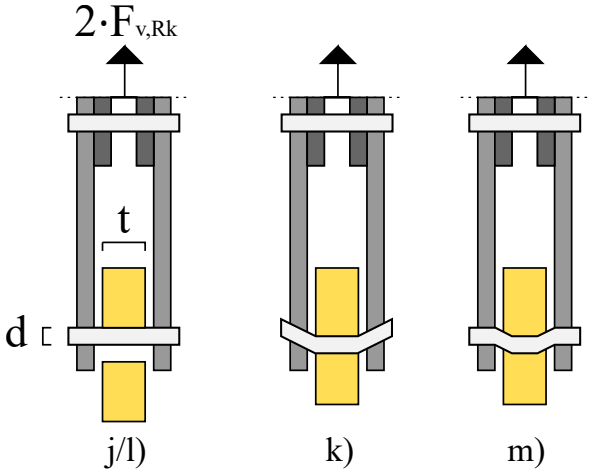

Figure 4.2: Failure mode j/l, k and m for dowel joints, inspired from [10]. Beam thickness (t) and dowel diameter (d) are shown. The joint capacity is $2 \cdot F_{v,Rk}$.

4.1 Embedment strength

According to Eurocode 5 [16], there are several ways a dowel joint could fail, four of them are of interest in this study. The desired failure modes are shown in figure 4.2. Case j and l is when embedment failure occurs. What differs j from k is the relation between the outer steel plates' thickness and the dowel diameter. The cases called m and k happen when the dowel is too weak or small in relation to the wood, meaning that the dowel will plasticise.

Cases j and l are thereby ideal when pure splitting is the aim of the tests, as the dowel will not yield. However, reaching case j and l is not the goal of the test since they are describing the embedment failure, not the pure splitting. To achieve pure splitting, the splitting capacity must be lower than case j and l, which in turn has to be lower than case m and k.

The minimum load in equation 4.1 and 4.2 would be chosen as a limiting value for characteristic capacity per shear plane. In this case, there are two shear planes shown in figure 4.2, hence the actual capacity of the joint is obtained by multiplying by two.

$$F_{v,Rk} = \begin{cases} j) 0.5 \cdot f_{h,90,k} \cdot t \cdot d \\ k) 1.15 \cdot \sqrt{2 M_{y,Rk} f_{h,90,k} d} + F_{ax,Rk}/4 \end{cases} \tag{4.1}$$

$$F_{v,Rk} = \begin{cases} l) 0.5 \cdot f_{h,90,k} \cdot t \cdot d \\ m) 2.3 \cdot \sqrt{M_{y,Rk} f_{h,90,k} d} + F_{ax,Rk}/4 \end{cases} \tag{4.2}$$

The input parameters for the calculations are the thickness of the wood, t, the dowel diameter, d, the characteristic embedded strength at a 90 degree angle from fibre direction, $f_{h,90,k}$, and the characteristic yield moment of the fastener, $M_{y,Rk}$. There is an option to take into account the extra added strength from the withdrawal of the fastener $F_{ax,Rk}$. The added strength is due to the head of the bolt putting pressure on the surface. Accounting this added strength would yield a higher capacity and it was therefore neglected since the lowest possible capacity is desired.

The loading was applied perpendicular to the grain and formula 4.3 was used to give the reduced embedment strength, compared to the full embedment strength when the loading is parallel to grain in formula 4.4.

$$f_{h,\alpha,k} = \frac{f_{h,0,k}}{k_{90} sin^2(\alpha) + cos^2(\alpha)} \tag{4.3}$$

The embedment strength is calculated from the dowel diameter and characteristic density, ρ_k. The scaling factor, k_{90}, which is based on hardwood, is also calculated. The embedment strength is calculated for a pre-drilled hole since a thick dowel is used. According to Eurocode 5, the following applies:

$$f_{h,0,k} = 0.082(1 - 0.01d)\rho_k \tag{4.4}$$

$$k_{90} = 0.90 + 0.015d \quad \text{(hardwood/birch)} \tag{4.5}$$

The characteristic yield moment, $M_{y,Rk}$, of a dowel fastener is calculated using the characteristic tensile strength, f_u, and the bolt diameter, d.

$$M_{y,Rk} = 0.3 f_u d^{2.6} \tag{4.6}$$

When the parameters are defined, the embedment strength can be calculated.

4.2 Bending capacity

To be assured that the beam is not too slender, resulting in a fracture by bending, the moment capacity needs to be checked. The expected failure load due to moment is calculated as:

$$F_{M,Rd} = \frac{4M_{Rd}}{l} \tag{4.7}$$

where the bending capacity, M_{Rd}, for the beam is calculated according to [10] as:

$$M_{Rd} = f_{m,k} \cdot W \cdot k_{crit} \tag{4.8}$$

Here, $f_{m,k}$ is the characteristic bending strength, and the section modulus $W = \frac{t \cdot h^2}{6}$, where t is the thickness of the beam and h is the cross section height. k_{crit} is a factor accounting for the effect of lateral buckling and is calculated as:

$$k_{\text{crit}} = \begin{cases} 1 & \text{for } \lambda_{\text{rel},m} \leq 0.75 \\ 1.56 - 0.75\lambda_{\text{rel},m} & \text{for } 0.75 < \lambda_{\text{rel},m} < 1.14 \\ \frac{1}{\lambda^2_{\text{rel},m}} & \text{for } 1.4 < \lambda_{\text{rel},m} \end{cases} \tag{4.9}$$

where $\lambda_{rel,m}$ is the relative slenderness ratio in bending:

$$\lambda_{rel,m} = \sqrt{\frac{f_{m,k}}{\sigma_{m,crit}}} \tag{4.10}$$

The critical bending stress $\sigma_{m,crit}$ is determined by using the 5^{th} percentile stiffness values:

$$\sigma_{m,crit} = \frac{\pi\sqrt{E_{0.05} I_Z G_{0.05} I_{tor}}}{l_{ef} W_y} \tag{4.11}$$

For a rectangular cross section of width t, height h, the moment of inertia about the weak axis $I_z = \frac{h \cdot t^3}{12}$ and the torsional moment of inertia $I_{tor} \approx \frac{t^3 \cdot h}{3}$, the equation for the critical bending stress, $\sigma_{m,crit}$, can be written with formula 4.11 as:

$$\sigma_{m,crit} = \frac{\pi \cdot t^2}{h \cdot l} \cdot \sqrt{E_{0.05} \cdot G_{0.05}} \tag{4.12}$$

Equation 4.12 is valid if the load is applied to the centroidal axis of the beam.

4.3 Dowel placement and requirements

To reach the ideal failure, the dowels have to be mindfully placed in the wooden beam [10]. In Eurocode 5, the dowel's distance to the beam edges are of importance to not obtain a brittle failure (splitting). Minimum requirements are therefore in place to ensure that the wood does not reach splitting failure before any other ductile mode. The minimum edge distance requirement, h_e, for loading perpendicular to the grain (α=90°) can be can be seen in figure 4.1 and it is calculated as:

$$h_e = max \begin{cases} (2 + 2 \cdot sin(\alpha))d = 4d \\ 3d \end{cases} \tag{4.13}$$

where d is the diameter of the dowel.

4.4 Splitting capacity

Wood is weak when loaded in tension perpendicular to the grain and the resulting failure mode is often cracking along the grain. This type of loading should be avoided, but it is not always possible, e.g. in a dowel-type connection. According to Eurocode 5 [10], the following condition should be satisfied if failure through spitting is to be avoided:

$$F_{v,Ed} \leq F_{90,Rd} \tag{4.14}$$

where

$$F_{v,Ed} = max \begin{cases} F_{v,Ed,1} \\ F_{v,Ed,2} \end{cases} \tag{4.15}$$

and where $F_{v,Ed,1}$ and $F_{v,Ed,2}$ are the design shear forces on either side of the connection. $F_{90,Rk}$ is the splitting capacity calculated according to equation 4.16, the formulation is only valid for softwoods in Eurocode 5 [10].

$$F_{90,Rk} = 14t\sqrt{\frac{h_e}{1 - \frac{h_e}{h}}} \tag{4.16}$$

Here h_e is the distance between the loaded edge and the center of the fastener, h is the height of the cross section of the beam and t is the thickness of the beam illustrated in figure 4.1.

Looking at equation 4.16 it seems as no consideration of the material properties such as strength or stiffness is taken. This is the result of a simplification made from the original equation [17] presented as :

$$F_{90,R} = t\sqrt{\frac{GG_c}{0.6}}\sqrt{\frac{h_e}{1 - \frac{h_e}{h}}} \tag{4.17}$$

where G is the longitudinal shear modulus and G_c is the critical energy release rate, which is assumed to correspond to the fracture energy G_f discussed in chapter 3. $F_{90.R}$ represents the shear force, which is later doubled to obtain the maximum force.

5 Method and material

The fracture energy can be experimentally determined by testing according to a method known as the Nordtest method. In this chapter, the method, preparation of the test specimens and the test setup is explained. To achieve the desired results, some adjustments to the method have been made. All changes are presented in this chapter.

The moisture content in the birch material is determined according to the Swedish standard EN 13183-1:2002 [18].

The test specimens were cut out from four different planks provided to this study. When the fracture energy of the wood was obtained, the remaining material from the original planks was was used for dowel joint tests. These tests were performed as 3-point bending tests, as described in section 5.2.

5.1 Test of fracture energy: The Nordtest method

Nordtest is a standard method for determining the fracture energy of wood in tension perpendicular to the grain (mode I), which is described in section 3.1. To achieve the objective of determining the fracture energy of a wood specimen, the following steps are taken in accordance with Nordtest method's NT Build 422 test manual [7].

5.1.1 Test setup

The test specimen was set up as a simply supported beam, as shown in figure 5.1. At one end, the beam rested on a steel prism on top of a steel ball, while the other end rested directly on a steel cylinder. The specimen was loaded with an constant rate of deflection set to 0.9 mm/minute. The loading was set at the midpoint, on top of another steel prism (shown in figure 5.1). A load deflection diagram was obtained by measuring the deflection, w, of the point load of the machine, and the load, F.

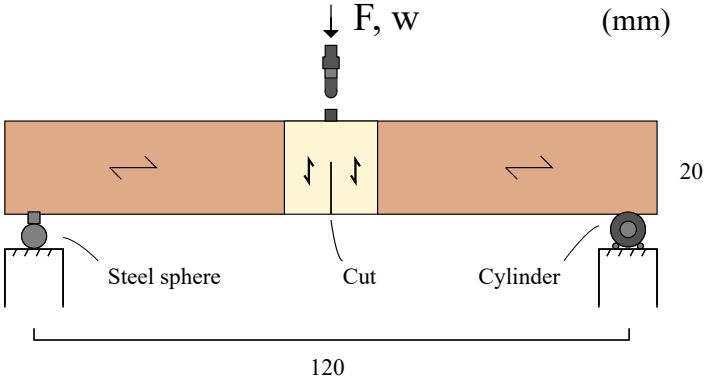

Figure 5.1: The 3-point bending test setup, inspired by the Nordtest method [7].

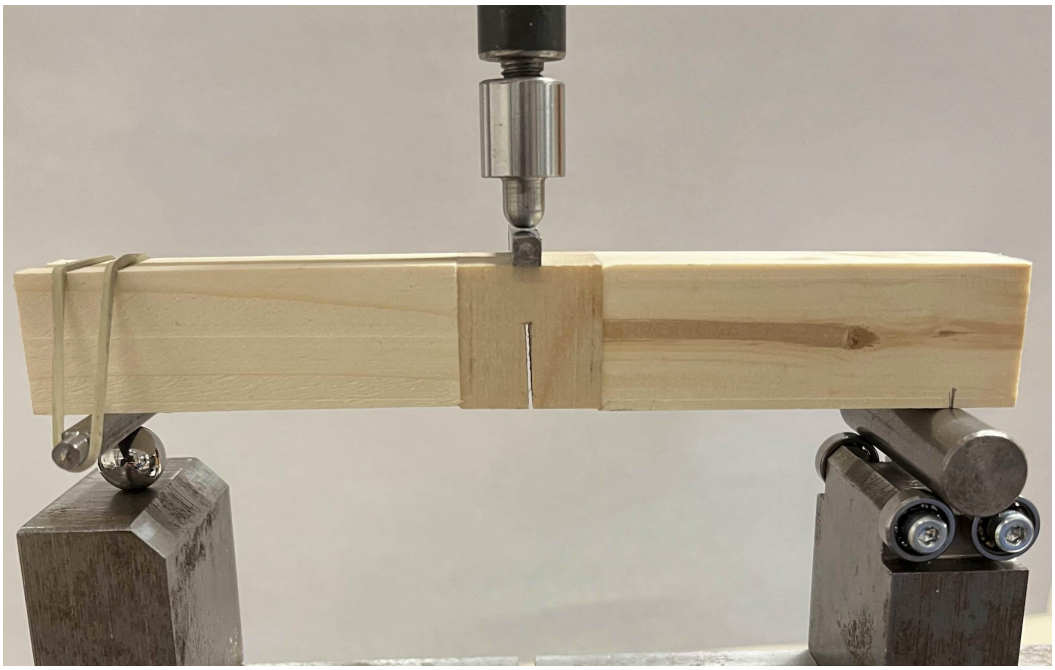

Figure 5.2: The real set-up based upon figure 5.1.

According to the Nordtest method [7], the entire test procedure, from the start to the collapse of the test specimen (i.e when the force applied to the test specimen F is equal to zero again), should proceed for 3±1 minutes. This was not implemented in this study where the tests proceeded for approximately 8 minutes.

5.1.2 Evaluation of fracture energy

The fracture energy, G_f, was calculated according to the Nordtest method [7] as:

$$G_f = \frac{W + mgw_0}{A_c} \tag{5.1}$$

where:

$$m = \frac{5}{6}m_{tot} + 2m_{prism} \tag{5.2}$$

and W is the work done by the midpoint force, F. W is the area under the load deflection curve seen in figure 5.3. The load-deflection curve was produced by using a linear regression function in MATLAB, including the post processing of the raw data. W was determined by numerical integration of the load deflection curve in MATLAB, using a trapezoidal function. The term, mgw_0, represents the work done by the dead weight and w_0 is the deflection when complete failure is obtained. The total mass of the test specimen, m_{tot}, and the weight of the steel prism, m_{prism}, resting on the test specimen was measured before the tests were conducted. Measurements were made with an accuracy of 0.01 g. A_c is the size of the fracture area defined in figure 5.9.

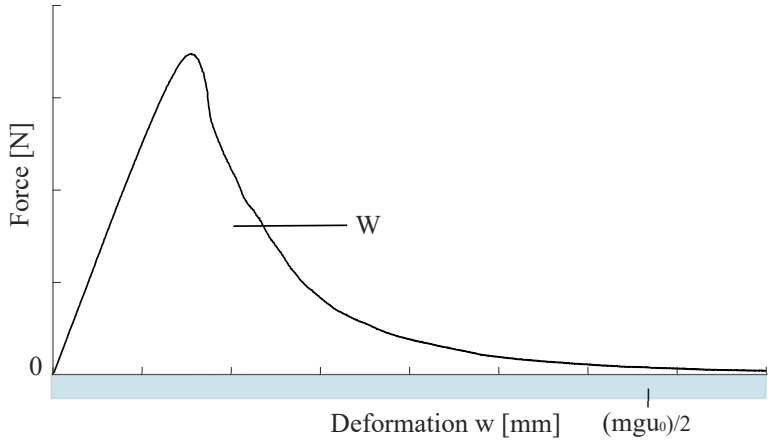

Figure 5.3: Schematic illustration of a load-deflection curve obtained from the experiments, inspired from [7]. The work, W, is denoted as the area.

5.1.3 Identifying stable and unstable responses

When conducting the experiments according to the Nordtest method, only stable responses should be considered as valid [7]. A way of analyzing the load-deformation curves is by introducing a restriction criterion, LC, by Forsman [12]:

$$LC = |F_i - F_{i+1}|/F_{max} \times 100 \tag{5.3}$$

where F_i and F_{i+1} are loads at two consecutive sample points and F_{max} is the maximum load capacity. The LC-value is thus a percent-value indicating the drop of the load-deformation curve. Different criteria for the LC can be introduced and compared. In [12], limits of 5%, 10%, 15% and 100% were investigated and the amount of accountable results, and how the results varied, was compared [12]. It was observed that choosing an LC value of 5 or 15 % did not impact the results significantly. Therefore the LC-value of 15% was used for the study.

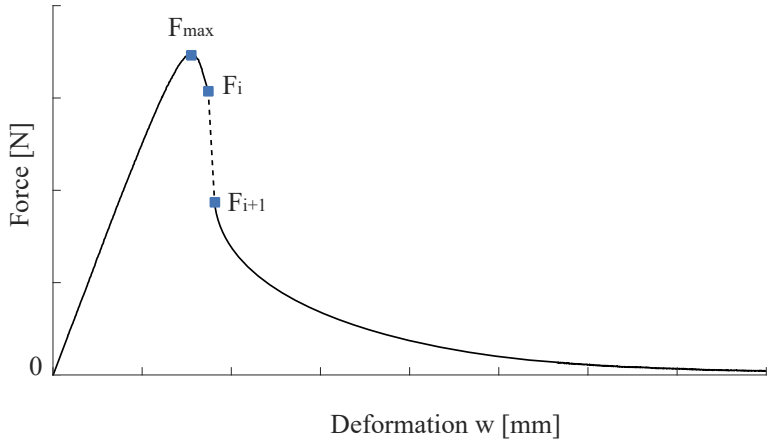

Figure 5.4: Load values, F, for different deformations. Figure is based on [12].

5.1.4 Preparation of test specimen

From the material provided, a stick was selected and cut out from every plank, with a dimension of 20×20 mm^2. From every stick, 10 cubes with a dimension of 20×20×20 mm^3 were extracted and numbered according to figure 5.5 and 5.6. The location of the stick was chosen so that the orientation of the annual growth rings would provide a fracture plane either in a pure RL or TL direction, as shown in figure 5.7.

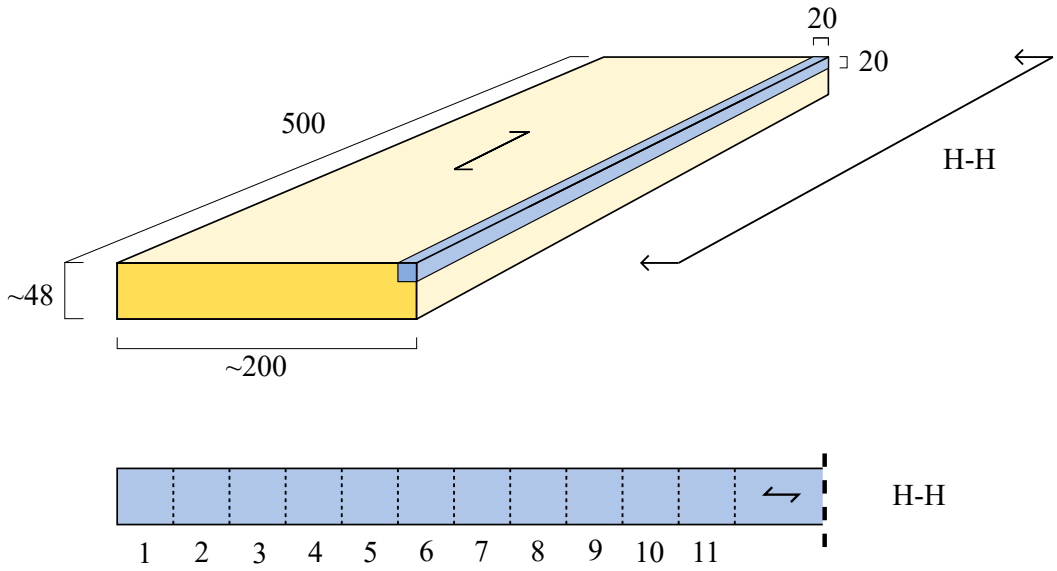

Figure 5.5: System of sawing and numbering the test cubes from each stick from each plank.

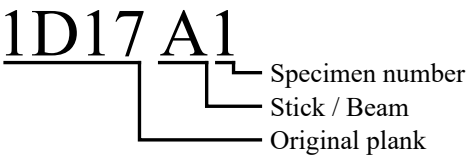

Figure 5.6: System of the numbering of the test cubes.

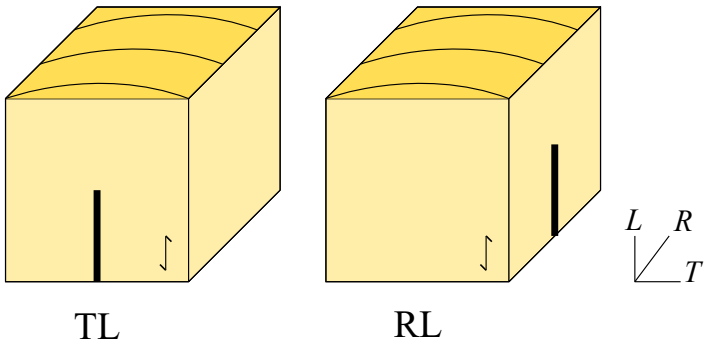

Figure 5.7: The RL and TL crack orientations. The thick line represents the sawn cut.

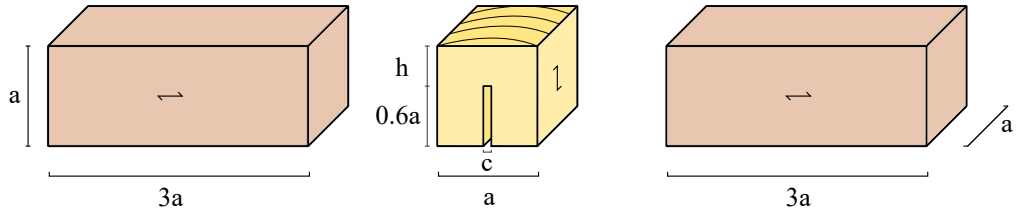

Figure 5.8: Dimensions for the birch specimen with a rectangular fracture area (middle) and the adjacent spruce parts. The grain direction and cut width, c, is defined. Here a = 20 mm and c = 0.7 mm.

Two of the 10 cubes, number 5 and 10 in figure 5.5, were tested for moisture content, see section 5.1.6. All of the samples were stored in a controlled climate where equilibrium is reached at a temperature of 20±2 °C and a relative humidity of 60±5%.

To achieve a more efficient usage of the Swedish birch provided to this study, the test cubes were glued together with two longer pieces made out of structural timber of strength class C24. The geometry of the complete beam is illustrated in figure 5.8, note that the test volume made of birch in the figure represent the geometry of a cube where a rectangular cut was used. The beams were then returned to the same controlled climate where the cubes first reached equilibrium. Here, the beams rest to let the glue properly harden. The beams were ready for testing when equilibrium was once again reached, which is when the weight does not differ by more than 0.1% after each weighing, which occurs every 24 hours.

According to standard SS-EN 408:2010+A1:2012 [19], when determining some physical and mechanical properties of wood, the test volume should not be outside a controlled climate more than one hour before testing. To ensure this, the testing of the specimens was done one at the time while the rest were stored in a tightly sealed plastic bag.

5.1.5 Geometry of test specimen

The test specimen consisted of three pieces, two longer wood pieces of C24 and a smaller test volume of birch, see figure 5.8. These parts were glued together to form a beam with the total length of 14 cm. The birch was oriented in two different directions, the TL or RL direction, see figure 5.7. Both orientations achieve a fracture plane oriented parallel to the grain. To induce the fracture in a desired spot, a notch was made at the bottom of the cube. The width of the notch was 0.7 mm and it was cut according to figure 5.8.

Different sawing blades leave different marks in the wood, which according to chapter 3 could influence the stress distribution in the cube. However, for the preparation of the cubes, the geometry of the cut was not documented. Moreover, the shape of the cut was assumed to be the same for all cubes.

Specimens with two different geometries for the fracture plane was tested, rectangular and triangular cross section, which are illustrated in figure 5.9.

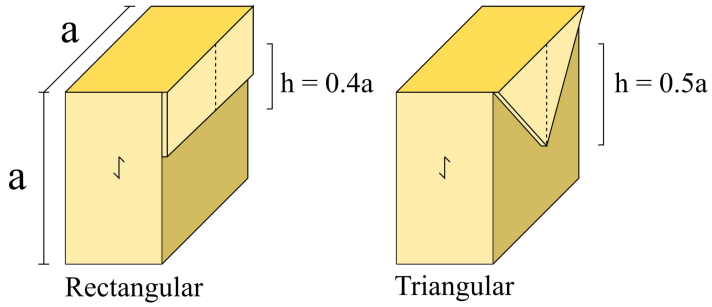

Figure 5.9: Triangular vs. Rectangular fracture area, inspired from [8]. The height of the fracture area h is marked in the centre of the cut side. Here $a = 20$ mm.

Rectangular area

The rectangular cross section produced mostly unstable fracture responses (defined in section 5.1.3) in the study by Lai and Plönning [8]. In [8] the notch height was 50% of the cube height. Instead, in this study the height of the sawn notch was 60% of the cube height, hoping to produce more stable responses.

Triangular area

For the tests reported in this study, the rectangular shape of the fracture plane provided unstable load-deflection curves for the first eight samples loaded in the RL direction. Therefore, the shape of the sawn notch was reevaluated, and for the remaining 16 specimens a triangular notch was used. The triangular shape of the notch has been used in earlier studies done by Forsman [12] and Lai and Plönning [8], with success. Note that a triangular fracture plane was used in both the TL and RL direction despite a rectangular plane being sufficient for producing stable results in the TL direction. In the end, the complete set of specimens had an equal amount of triangular and rectangular fracture planes. For the triangular fracture areas, the height of the notch was set to 50% of the cubes' height, since it simplified the production.

5.1.6 Density and moisture content

The density, ρ (kg/m^3), of the test volume was determined by equation 5.4, where m_u is the weight of the test volume when it has reached equilibrium at 60% RH and 20°C. The definitions of the measurements of the test volume is defined in figure 5.10. The measurements are made after equilibrium is reached.

$$\rho_u = \frac{m_u}{a \cdot b \cdot l} \tag{5.4}$$

Two cubes (number 5 and 10) from every plank were tested for moisture content with the oven-dry method according to SS-EN 13183-1 [18]. The location from where these cubes were extracted is shown in figure 5.5. Since the weight of the test volume was less than 100 g, the weight was determined with an accuracy of 0.01 g according to the standard. After the test cubes reached equilibrium at 60% RH and 20 °C, they were dried at 105 °C over a period of time until the change of weight was less than

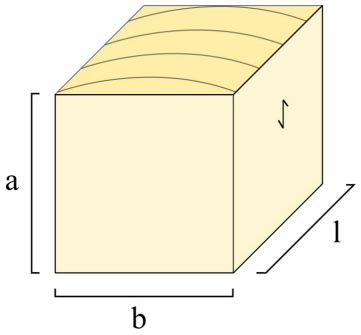

Figure 5.10: Measurements of the cube.

0.1% after weighing every other hour. The moisture content, u, was then calculated according to:

$$u = \frac{m_1 - m_0}{m_0} \cdot 100 \tag{5.5}$$

Where u (%) is the moisture content, m_1 is the weight of the test cube before drying and m_0 is the weight of the test cube after drying. The calculated moisture content and density for the test specimens are presented in table 5.1.

Table 5.1: Density and moisture content for the test specimens.

	Density [kg/m^3]			**Moisture content [%]**		
Specimen ID	**Number of specimens**	**Mean value**	**CoV [%]**	**Number of specimens**	**Mean value**	**CoV [%]**
1D17A	10	646.0	1.0	2	11.5	0.1
1D19A	10	682.9	1.1	2	12.4	0.1
1D20A	10	608.7	1.2	2	11.9	0.0
1D21A	10	652.2	5.0	2	12.2	0.1
Total:	**40**	**647.5**	**5.3**	**8**	**12**	**3.0**

5.1.7 Adjustments of the Nordtest method

According to Nordtest [7] the load with the fixed rate of the displacement should be 2 mm/minute. This was changed to 0.9 mm/minute. The reason was that unstable results appeared for specimens with a fracture plane in the RL direction and with a rectangular fracture area.

The volume of the samples in this dissertation depart from the dimensions given in the Nordtest method. Earlier studies [8, 12] have been conducted using the same sample dimensions as in this dissertation. The test specimen volume was only 1/3 of the suggested dimensions by Nordtest [7]. Therefore, the size and weight will be measured with a accuracy of 0.01 mm^2 respectively 0.1 g.

The support conditions used in the test setup were slightly modified after four specimens had been tested. There was a tendency for the specimen to fall off of the

supports before a collapse of the beam was achieved, i.e before the force was equal to zero. The downward deflection resulted in an additional displacement in the horizontal direction, leading to the prism falling of the cylinder. This was solved by changing the steel cylinder to a bigger dimension, leading to the beam only having to rest on one prism and sphere instead of two. The modified setup is shown in figure 5.1. The change of support leads to a higher stress concentration, since the cylinder has a smaller contact surface than the prism. No additional visible deformation was observed on the test specimen due to this change.

5.2 Joints

In this section, the experimental testing of the splitting capacity of the dowel joints is explained. The aim is to determine whether the fracture energy obtained from the tests presented in section 5.1 could be used to predict the dowel joints' capacities.

5.2.1 Test setup

The method for testing the dowel joints was done in accordance with Forsman [12]. Three-point loading, with the load applied in the center of the beam with respect to the beam length direction, was used.

The experimental testing makes use of two supports located at a distance of 0.45 m from each other (L). The boundary condition was assumed to give allowance for rotation, but without twisting. The placed dowel, in accordance with chapter 4.3, was attached to the MTS machine. The MTS machine had a set rate of displacement at 1 mm/min upwards. The force and displacement was recorded. The maximum force recorded was then compared to the calculated value in section 5.2, which was based on the fracture energy, G_f, determined from the tests presented in section 5.1.

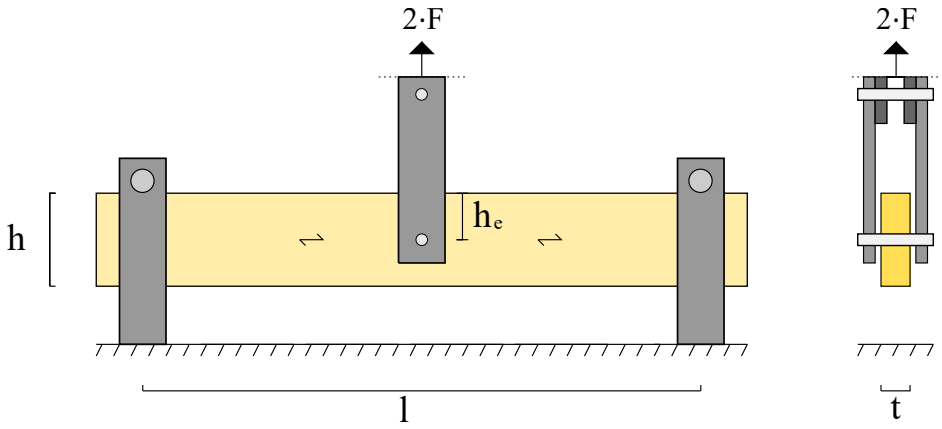

Figure 5.11: Beam setup for failure mode testing, inspired from [12]. The minimum distance h_e is in relation to the edge subjected to pressure.

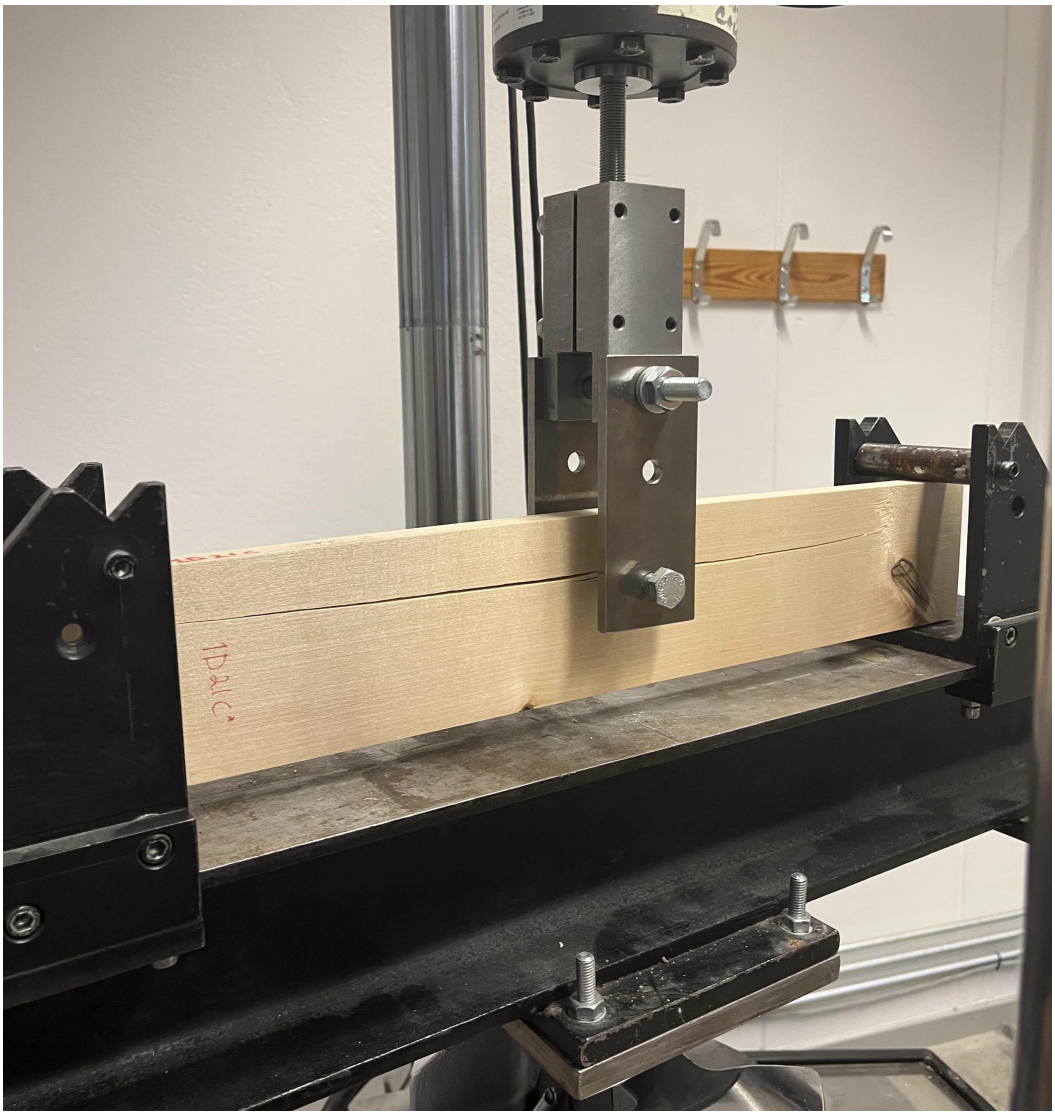

Figure 5.12: The test-setup for the dowel tests.

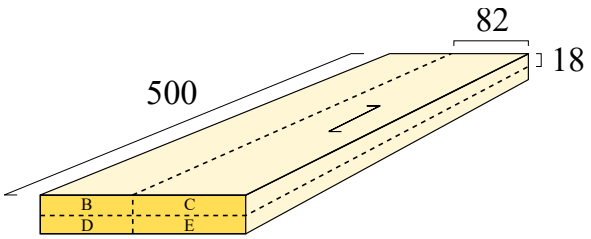

Figure 5.13: System of numbering the beams, e.g. 1D17B. Units are in mm.

5.2.2 Preparation of test specimen

From the material provided to this project, 13 beams with a dimension of 500×82×18 mm were sawn. The numbering of the beams was made according to the same system as in section 5.1.4, as shown in figure 5.13. The beams were stored in a climate chamber, with a constant temperature at 20±2 °C and a relative humidity of 60±5% until they reached equilibrium. Just before the beams were tested, a hole with a diameter of $d = 10$ mm was made in the desired position. The edge distance from the centre of the hole to the loaded edge should, according to Eurocode 5 and section 4.3, be at least $4d$.

When the first four beams had been tested, the edge distance was reevaluated since the desired result of pure splitting was not obtained. Therefore, only seven of the beams (1D17B-E, 1D19B, 1D20B and 1D20D) were designed according to the requirements in Eurocode 5. The remaining beams (1D20C, 1D20E and 1D21B-E) were modified by instead using an edge distance of $3d$.

5.2.3 Calculation of joint strength

The formulas and guidelines from Eurocode 5, described in chapter 4, were used for estimating the outcome for the dowel testing. The dowel placement was altered from $h_e = 4d$ to $3d$ for some beams, making the desired outcome of pure splitting more likely.

The shear modulus for this material is not known, therefore an estimated value was used based on results from previous experiments presented in [9]. The shear modulus, G, is set to 910 MPa in the TL direction and 1180 MPa in the RL direction.

6 Results - fracture energy in birch

6.1 Fracture area

The triangular and rectangular fracture area were measured after the tests were conducted, and the average values are presented in table 6.1. The fracture areas were measured using a photo editing software, where first the size of one pixel was determined and then the number of pixels covering the fracture area were counted. The measured fracture area for every individual piece is tabulated in table A.2 in appendix A.

Table 6.1: Tabulated average fracture areas for each series: Triangular (Tri) vs. Rectangular (Rec). The combined average for triangular and rectangular is also given with the respective CoV.

Specimen ID	Shape of notch	Avg. Fracture area [mm^2]	Combined avg. fracture area [mm^2]	CoV [%]
1D19A	Rec	160.3	160.7	3.7
1D20A	Rec	161.1		
1D17A	Tri	82.8	82.2	4.4
1D21A	Tri	81.6		

6.1.1 Observations of fracture area size

It is shown in table 6.1 that the average specimen, from each test series, has a similar cross section area when comparing the triangular sections or the rectangular sections. The coefficient of variation (CoV) for the triangular cross section was 0.7 per-cent units higher than the CoV for rectangular cross section. The variation may be explained by the cubes' varying dimensions, with the side lengths not being exactly 20 mm. It could also be due to small inaccuracies in the cutting-stage, since holding the samples by hand, while utilizing the bandsaw, is not stable compared to a machine.

6.2 Loads and deflections for RL and TL directions

Examples of the experimentally determined responses, in terms of load (F) and deflection (w), are shown in figures 6.1 and 6.2. The illustrations in figure 6.1 show a typical behavior of the specimens in series 1D17A and 1D21A, representing the triangular fracture area for both RL and TL directions. A typical behavior for series 1D19A and 1D20A, representing the rectangular fracture area for both RL and TL directions, is shown in figure 6.2. In table 6.2, the shape of the notch, the orientation of the notch in relation to the direction of the annual growth rings, the density, maximum load, calculated fracture energy and whether a stable or unstable response was

obtained is reported for every specimen. An unstable response is obtained when the load decreases momentarily at some instant during the test, according to Nordtest [7]. According to section 5.1.3, an LC value of 15% was used.

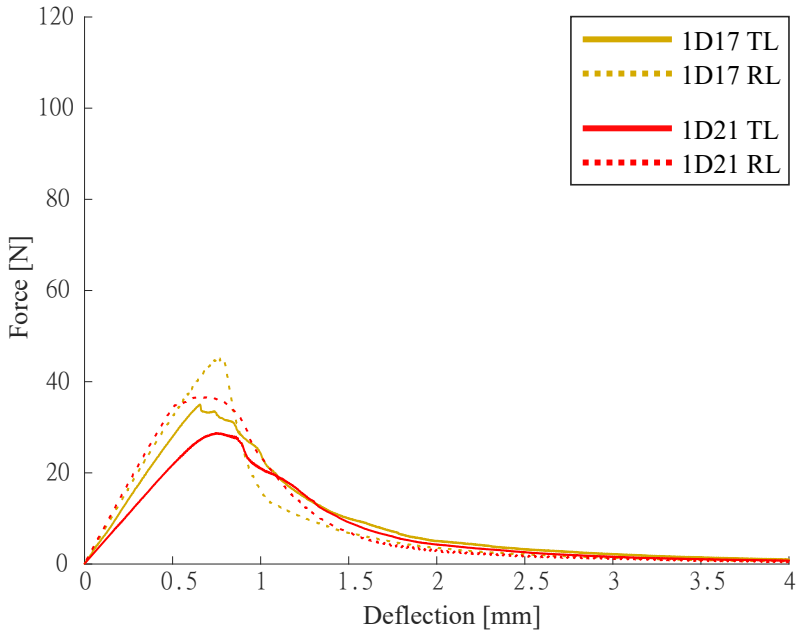

Figure 6.1: Illustration of a typical load deflection response for specimens with a triangular fracture area.

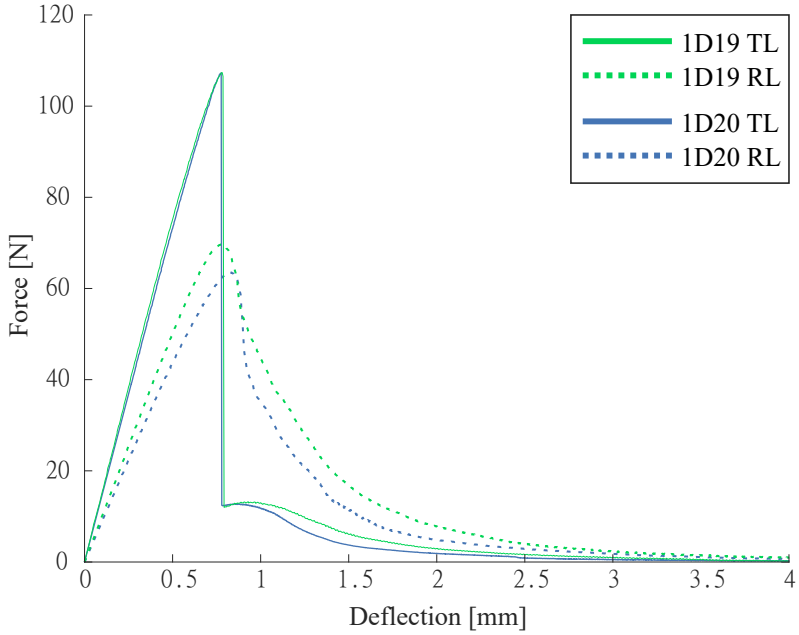

Figure 6.2: Illustration of a typical load deflection response for specimens with a rectangular fracture area.

Table 6.2: Test result and calculated fracture energy, G_f for test specimen.

Specimen ID	Shape of notch	Orientation	Density [kg/m^3]	Max load [N]	G_f [J/m^2]	Stable curve
Series 1D17A						
1D17A2	Tri	RL	640.1	35.6	471.4	x
1D17A4	Tri	RL	660.4	49.7	486.6	x
1D17A9	Tri	RL	644.9	38.5	429.3	x
1D17A11	Tri	RL	649.1	45.0	456.7	x
1D17A1	Tri	TL	645.6	35.1	517.1	x
1D17A3	Tri	TL	639.0	28.3	550.7	x
1D17A6	Tri	TL	648.7	35.0	471.8	x
1D17A8	Tri	TL	644.8	34.8	453.3	x
Series 1D19A						
1D19A2	Rec	RL	668.1	107.8	316.8	
1D19A4	Rec	RL	681.1	107.4	373.5	
1D19A7	Rec	RL	690.3	100.0	380.2	
1D19A9	Rec	RL	687.7	115.2	395.8	
1D19A1	Rec	TL	678.1	77.5	448.8	x
1D19A3	Rec	TL	674.4	62.7	400.4	x
1D19A6	Rec	TL	685.8	63.7	395.7	x
1D19A8	Rec	TL	693.4	69.6	424.5	x
Series 1D20A						
1D20A2	Rec	RL	614.1	111.0	388.6	
1D20A4	Rec	RL	612.0	110.0	343.4	
1D20A7	Rec	RL	607.6	107.2	327.8	
1D20A9	Rec	RL	595.0	101.8	333.5	
1D20A3	Rec	TL	616.4	65.2	302.0	
1D20A6	Rec	TL	609.0	68.0	410.3	x
1D20A8	Rec	TL	601.3	63.5	346.6	x
1D20A11	Rec	TL	618.8	65.5	420.7	x
Series 1D21A						
1D21A2	Tri	RL	657.3	36.6	466.5	x
1D21A4	Tri	RL	722.7	47.5	563.2	x
1D21A7	Tri	RL	635.5	38.6	417.9	x
1D21A9	Tri	RL	624.1	37.7	443.6	x
1D21A1	Tri	TL	634.1	28.6	390.4	x
1D21A3	Tri	TL	683.7	29.8	459.8	x
1D21A6	Tri	TL	635.9	23.8	427.9	x
1D21A8	Tri	TL	628.4	24.7	403.4	x

6.2.1 Observations of loads and deflections

In the description of the Nordtest method [7], it is stated that the load deflection response must be stable for the result to be valid, see section 5.1.3 for definition of a stable result. Examples of unstable responses are observed in figure 6.2, where two series with a rectangular fracture area are shown. In the figure, showing the result of

the loading in TL and RL directions, the RL has the steeper (unstable) response after reaching its maximum load. Table 6.2 presents that 8/8 specimens with rectangular fracture area, loaded in RL direction, showed an unstable response. This means that 25% of the total sample size are invalid, according to the set LC-value of 15%. It also means that 50% of the responses in the RL direction are invalid. Table 6.3 summarizes the maximum load for the stable and unstable responses, with the crack orientation in the RL direction.

Only one of the specimens with a rectangular fracture areas showed an unstable response in the TL direction. Contrary, the triangular fracture areas yielded only stable responses, as seen in table 6.2. Figure 6.1 shows an example of the obtained stable responses for both the RL and TL direction, with a triangular fracture area. Table 6.4 shows a summary of table 6.2 for the cubes tested in the TL direction.

It is seen that the cubes with a crack propagation in the RL direction, in table 6.3, withstand a higher load than the ones in the TL direction, seen in table 6.4.

Observing the specimens loaded in TL direction, presented in table 6.4, the maximum force is 55% lower for the specimens with a triangular fracture area compared to specimens with a rectangular fracture area. The maximum load had a bigger CoV when a triangular fracture area was used, compared to when using a rectangular one, which is also shown in table 6.4. Comparing the CoV of the maximum loads in tables 6.4 and 6.3 to the CoV for the fracture area in table 6.1, specimens with a triangular fracture area showed a higher CoV for the size of the area than specimens with a rectangular fracture area. This might indicate that the size of the area effect the maximum load more when a triangular shaped notch is used, compared to when a rectangular shape is used. This could be due to the stress distribution being different for the different geometries [8].

Table 6.3: Max load for RL direction.

	Rectangular shape		**Triangular shape**	
Type of response	**Max load [N]**	**CoV [%]**	**Max load [N]**	**CoV [%]**
Stable	-	-	41.1	13.2
Unstable	107.5	4.5	-	-

Table 6.4: Max load for TL direction.

	Rectangular shape		**Triangular shape**	
Type of response	**Max load [N]**	**CoV [%]**	**Max load [N]**	**CoV [%]**
Stable	67.2	7.7	30	15.2
Unstable	65.2	-	-	-

6.3 Fracture energy

Table 6.5 and 6.6 show the specimens' calculated fracture energy based on the measured load, deflection and fracture area for each test cube from section 6.1 and 6.2. Only the specimens with a stable response are of interest when calculating the average fracture energy for the material (since the sudden drop in the load displacement curve creates some uncertainty about the behavior of the specimen). The fracture energy is calculated according to section 5.1.2. The stable maximum and minimum fracture energies from table 6.2 are shown in table 6.7 for both the RL and TL directions.

Table 6.5: Fracture energy for RL direction.

	Rectangular shape		**Triangular shape**		**Rectangular and triangular shape**	
Type of response	**G_f [J/m^2]**	**CoV [%]**	**G_f [J/m^2]**	**CoV [%]**	**G_f [J/m^2]**	**CoV [%]**
Stable	-	-	466.9	9.2	466.9	9.2
Unstable	357.5	8.5	-	-	357.5	8.5

Table 6.6: Fracture energy for TL direction.

	Rectangular shape		**Triangular shape**		**Rectangular and triangular shape**	
Type of response	**G_f [J/m^2]**	**CoV [%]**	**G_f [J/m^2]**	**CoV [%]**	**G_f [J/m^2]**	**CoV [%]**
Stable	406.7	7.8	459.2	11.9	434.8	11.8
Unstable	302.0	-	-	-	302.0	-

Table 6.7: The maximum and minimum fracture energy in the RL direction and the TL direction for the stable responses in table 6.2. An average is also presented for the respective direction.

Variable	**Value**	**Avg. Value**	**Unit**
$G_{f,RL,min}$	417.9	466.9	J/m^2
$G_{f,RL,max}$	563.2		
$G_{f,TL,min}$	346.6	434.8	
$G_{f,TL,max}$	550.7		

6.3.1 Density and fracture energy

Figure 6.3 and 6.4 show the relation between the measured density and the obtained fracture energy for the specimens. The correlation coefficient is 0.40 for all of the results in figure 6.3, and 0.43 for the stable results in figure 6.4, both suggesting a moderately positive correlation between fracture energy and density.

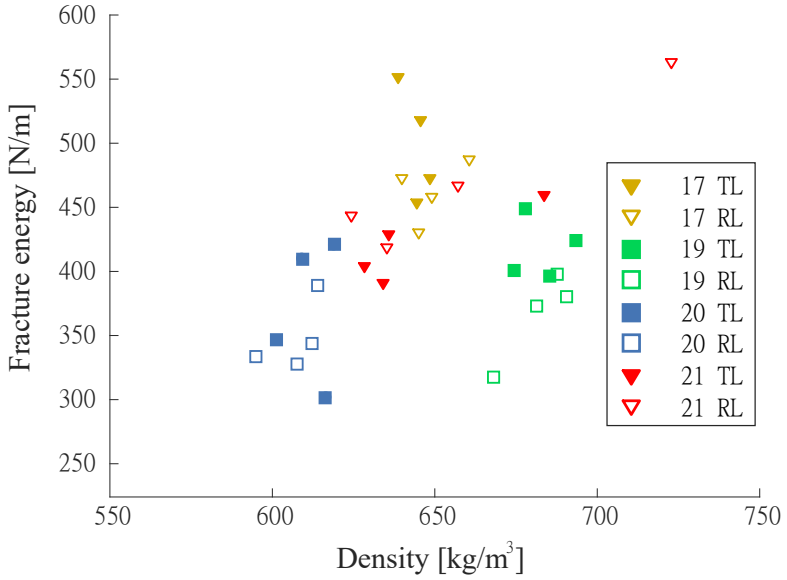

Figure 6.3: Fracture energy for different stable and unstable responses from series (-17, -19, -20 and -21), cross sections and densities.

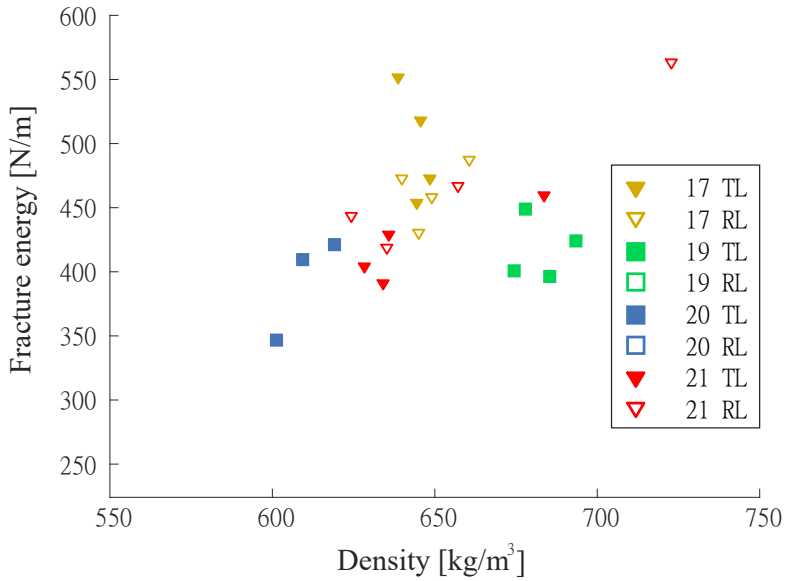

Figure 6.4: Fracture energy for different stable responses from series (-17, -19, -20 and -21), cross sections and densities.

6.3.2 Observations of fracture energy

Looking at tables 6.5 and 6.6, the RL direction shows a 7% higher fracture energy compared to the TL direction, but when looking only at the specimens with a triangular fracture area, the difference in fracture energy is only 1.7 %. Looking at the series with a triangular fracture area (1D17 and 1D21), which showed stable responses for both RL and TL direction, there is a difference where one series showed a higher fracture energy in the TL direction over the RL direction. This is the opposite when comparing to the other series. Series 1D17 has a mean fracture energy of 461.0 J/m^2 in the RL direction and 498.2 J/m^2 in the TL direction. Series 1D21 had a mean fracture energy of 472.8 and 420.4 J/m^2 in the RL and the TL direction, respectively.

An explanation to the low fracture energy in the RL direction, compared to the TL direction, could be that the method and system used for sawing out the cubes gives that the same annual growth rings passes through the cubes. For the cubes with the crack propagation oriented in the RL direction, the likelihood that the fracture happens in the same annual growth ring is high. There is a possibility that we encountered a weak year, meaning a year when the growth conditions for the tree was not as advantageous (e.g. series 1D17). When the fracture is oriented in the TL direction, the impact of a weak year should be of much less influence since the crack propagates over several annual growth rings.

Studying the relation between the density of the specimens and the fracture energy, in figure 6.4, a linear relationship might be observed. A denser material could indicate that it has a higher portion of fibres relative to the volume occupied by vessels, than a less dense material. A wood piece with a higher amount of fibers is often also stronger, compared to a piece with less fibres, according to [9]. This statement correlates with the observations made in this study. In series 1D21, one of the cubes had a much higher density than the rest of the samples. This could indicate that there was some kind of abnormality or knot in this part of the wood. This cube had a higher fracture energy, which also correlates with earlier statement.

7 Results - dowel joint

This chapter presents the results of experimental dowel-type joint tests. The test setup and specimen geometry was designed so that the failure would be either embedment failure in the wood or a brittle failure by cracking. When designing a real structure, failure due to yielding of the dowels is generally preferred.

7.1 Calculated capacity of dowel joint

When estimating the capacity of the beam, using Eurocode 5 according to chapter 4, using the correct material data is essential. However, not all of the necessary material parameters are known for the birch. In table 7.1, the used material parameters are presented. The density, presented in table 7.1, is the 5^{th} percentile of the measured density for the test cubes in table 5.1. The critical energy release rate, G_c, is chosen as the mean value from the stable fractures in table 6.5 and 6.6. Note that G_c and G_f are assumed to be equivalent. Since there is no available data for the shear modulus for this specific material, an assumption on the safe side has been made. The mean shear modulus, G, used for calculating the bending capacity, is assumed to be the mean value of the G_{RL} and G_{TL}, gathered from [9]. There are some variation in the geometry of the beams, the mean values of these variations are presented in table 7.2.

Table 7.1: Material parameters used when calculating the capacity of the dowel joint.

Parameter name	Variable	Value	Unit	Source
Characteristic density	ρ_k	595	kg/m^3	Table 5.1
Fracture energy (Avg)	$G_{c,RL}$	467	J/m^2	Table 6.5
	$G_{c,TL}$	435	J/m^2	Table 6.6
Elastic modulus	$E_{0.05}$	5000	MPa	[6]
Bending capacity || fibre	f_m	60	MPa	[6]
Shear modulus	G	1045	MPa	[9]
	G_{TL}	910	MPa	[9]
	G_{RL}	1180	MPa	[9]

Table 7.2: The mean dimensions of the beams used when calculating the capacity.

Parameter name	Variabel	Value	Unit
Thickness	t	18	mm
Height of beam	h	82	mm
Length between support	l	450	mm
Diameter of hole	d	10	mm

7.1.1 Calculated embedment strength

The theoretical joint capacity, F_{vRk}, of the beam was calculated according to section 4.1. The results of these calculations are presented in table 7.3, using the material parameters in table 7.1. According to Svenskt Trä [10], different failures could occur in dowel-type connections. The sought failure for this study is either case j) or l), shown in figure 4.2. The calculations predicts that there will be an embedment failure in the wood, $F_{v,Rk,j}$ or $F_{v,Rk,l}$, before the dowel plasticises. The capacity, presented in table 7.3, is valid for two shear planes and the capacity of the beam is approximately 7.4 kN, according to chapter 4.

Failure mode j) and k) or l) and m) are considered with respect to the outer steel plates' thickness. All possible outcomes are shown.

The M8.8 dowel, that was used in the test, had a yield capacity of 640 MPa and a diameter of 10 mm. The dowel diameter was the same as the diameter for the pre-drilled hole.

Table 7.3: Calculated joint capacity according to chapter 4.1.

Parameter name	Variable	Value	Unit	Equation
Yielding capacity for M8.8	$M_{y,Rk}$	76437	Nmm	4.6
Scaling factor	k_{90}	1.05	-	4.5
Embedment strength || grain	$f_{h,0,k}$	43.9	MPa	4.4
Embedment strength $\perp$ grain	$f_{h,90,k}$	41.8	MPa	4.3
Calculated joint capacity				
Shear capacity (two shear planes)	$2 \cdot F_{v,Rk,j}$	7400	N	4.1
	$2 \cdot F_{v,Rk,k}$	18400	N	4.1
	$2 \cdot F_{v,Rk,l}$	7400	N	4.2
	$2 \cdot F_{v,Rk,m}$	26000	N	4.2

7.1.2 Calculated bending capacity

The bending capacity of the beam was calculated according to section 4.2, with material parameters presented in table 7.1 and 7.2. When calculating the predicted bending capacity of the beam, an average bending strength, f_m, was used instead of the characteristic in order to achieve the most accurate value. The theoretical capacity with respect to bending, $F_{M,Rd}$, of the beam is calculated to 10.6 kN, presented in table 7.4.

7.1.3 Calculated splitting capacity

The splitting capacity, $2 \cdot F_{90,Rk}$, of the beam was calculated according to section 4.4, using the fracture energy presented in table 7.1. The fracture energy was experimentally obtained according to chapter 5.1. Table 7.5 shows the calculated splitting capacity, using the mean shear modulus ($G = 1045$ MPa) and mean fracture energy for the RL ($G_{c,RL} = 467$ J/m^2) and TL ($G_{c,TL} = 435$ J/m^2) directions.

Table 7.4: Calculated bending capacity.

Parameter name	Variable	Value	Unit	Equation
Critical bending stress	$\sigma_{m,crit}$	52.8	MPa	4.12
Relative slenderness	λ	0.4	-	4.10
Lateral buckling factor	k_{crit}	1.0	-	4.9
Section modulus	W	$19.8 \cdot 10^{-6}$	m^3	Chapter 4.2
Bending capacity	M_{Rd}	1190	Nm	4.8
Failure load due to moment	$F_{M,Rd}$	10.6	kN	4.7

Table 7.5: Calculated splitting capacity.

Parameter name	Variable	h_e/h	Value	Unit	Equation
Splitting strength	$2 \cdot F_{90,R}$	0.37	6824.0	N	7.1
		0.49	8767.7	N	7.1

7.1.4 Observations of calculations

The test setup and the specimen geometry was designed to promote a brittle failure. This means that the calculated capacity of the splitting force should be the lowest capacity out of the different failures discussed above. When an edge distance of $3d$ was used, i.e $h_e/h = 0.37$, the predicted failure would be due to splitting. When using a edge distance of $4d$, $h_e/h = 0.49$ the predicted failure would instead be an embedment failure.

When observing the equation for splitting capacity, equation 7.1, the formulation can be simplified by inserting the values for the assumed shear modulus, G, and mean fracture energy, G_c. When G and G_c are gathered from table 7.1, the following simplification is made:

$$F_{90,R} = t\sqrt{\frac{GG_c}{0.6}}\sqrt{\frac{h_e}{1-\frac{h_e}{h}}} \tag{4.17}$$

becomes

$$F_{90,R} = 28t\sqrt{\frac{h_e}{1-\frac{h_e}{h}}} \tag{7.1}$$

which can be compared to the formula for softwoods

$$F_{90,Rk} = 14t\sqrt{\frac{h_e}{1-\frac{h_e}{h}}} \tag{4.16}$$

Comparing the simplified equation of 7.1 to equation 4.16, which has a coefficient of $14t$, the formulation suggests that the birch has twice the splitting capacity compared the characteristic splitting capacity of softwood. Note that average, not characteristic,

shear modulus and fracture energy have been used to calculate the birch's splitting capacity. This is further discussed and illustrated in section 7.2.3.

7.2 Experimental results

Here, the experimental results for the dowel-type joint tests and the measured load-deflection responses are presented. It can be seen in figures 7.1 and 7.2 that the joints with an edge distance of $4d$ withstand higher loading in general, before splitting failure.

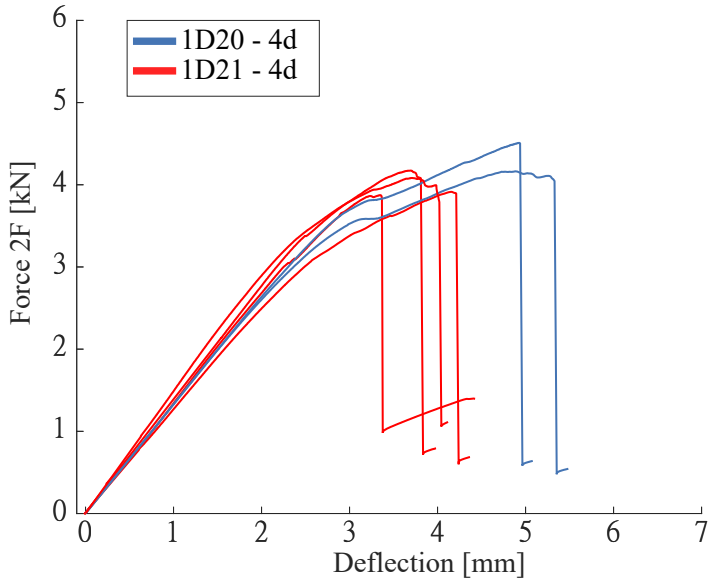

Figure 7.1: The load-deflection relation for all dowel tests. Dowel edge distance was $3d$, where d is dowel diameter.

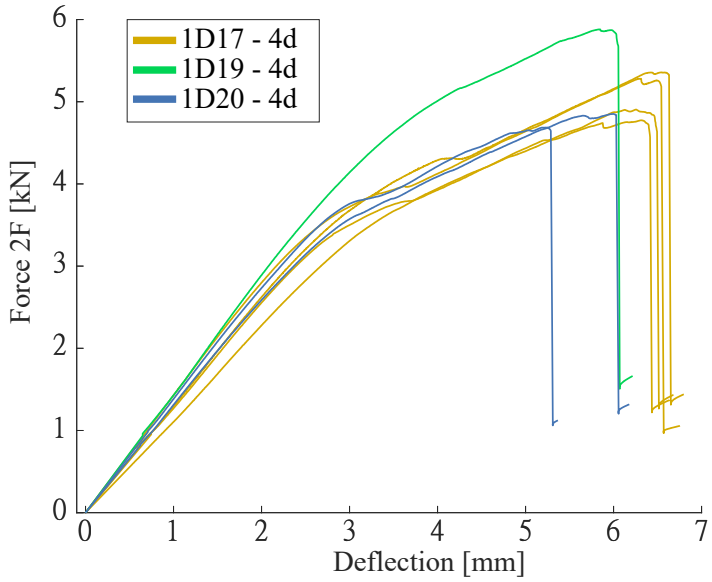

Figure 7.2: The load-deflection relation for all dowel tests. Dowel edge distance was $4d$, where d is dowel diameter.

Table 7.6: Test results for dowel joint tests, measured deformation and angle between the crack and the annual growth rings.

Beam ID	Density [kg/m^3]	h_e/h	Embedment deformation [mm]	Max load 2·F[N]	TL-RL ratio
Series 1D17					
1D17B	639.5	0.49	1.14	4905	0.36
1D17C	640.0	0.49	1.66	5281	0.67
1D17D	623.5	0.49	1.33	5358	0.58
1D17E	624.8	0.49	1.15	4775	0.50
Series 1D19					
1D19B	639.3	0.49	0.80	5881	0.82
Series 1D20					
1D20B	591.3	0.49	1.14	4852	0.72
1D20C	579.0	0.37	1.17	4164	0.61
1D20D	594.5	0.49	1.22	4687	0.94
1D20E	579.4	0.37	0.66	4510	1.00
Series 1D21					
1D21B	593.6	0.37	0.64	3922	0.71
1D21C	609.3	0.37	0.60	4083	0.83
1D21D	604.1	0.37	0.47	3883	1.00
1D21E	596.3	0.37	0.46	4181	0.92

Table 7.6 shows the density for each beam, the maximum load and the ratio h_e/h, which is the the dowel placement from the loaded edge divided by the beam height. The embedment deformation is defined as the difference between the deformed and the initial pre-drilled dowel hole, which deformed in the load (F) direction (perpendicular to grain). The deformations were measured with a caliper when the beam was detached from the test setup. The values are not entirely accurate and should only be seen as an approximation. The presented TL-RL ratio is based on the angle between the crack plane and the annual rings, defined as $\cos(\alpha)$ in figure 7.3. A ratio of 0.0 is pure TL cracking and 1.0 is pure RL cracking. This measurement is only made at the beam-ends.

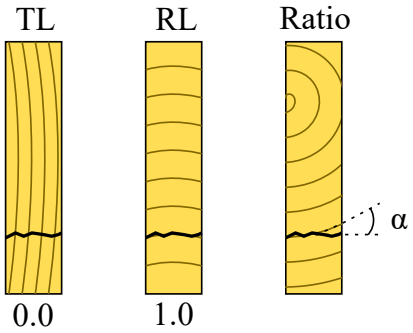

Figure 7.3: The TL-RL ratio - the angle between the crack and the annual growth rings.

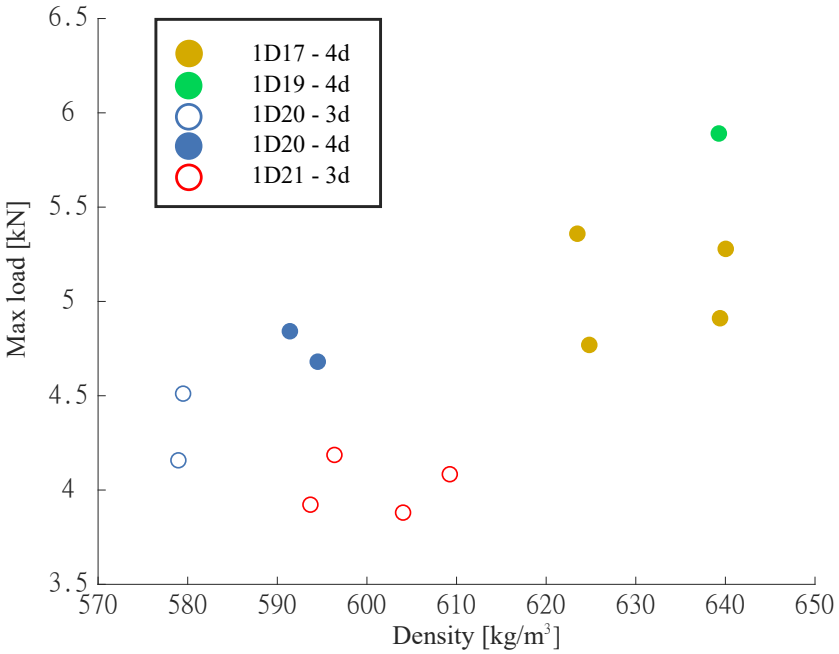

Figure 7.4: Density and maximum load for each beam for edge distances $3d$ (circles) and $4d$ (filled circles).

In figure 7.4, the density, edge distance and maximum load is presented for each tested beam.

In figure 7.5 the maximum load is depicted in relation to the TL-RL ratio. Here, 0 is pure TL oriented fracture and 1 is a purely RL oriented fracture.

Figure 7.6 shows the relation between the embedment deformation, i.e the deformation that was measured in the pre-drilled hole, and the maximum load for each beam.

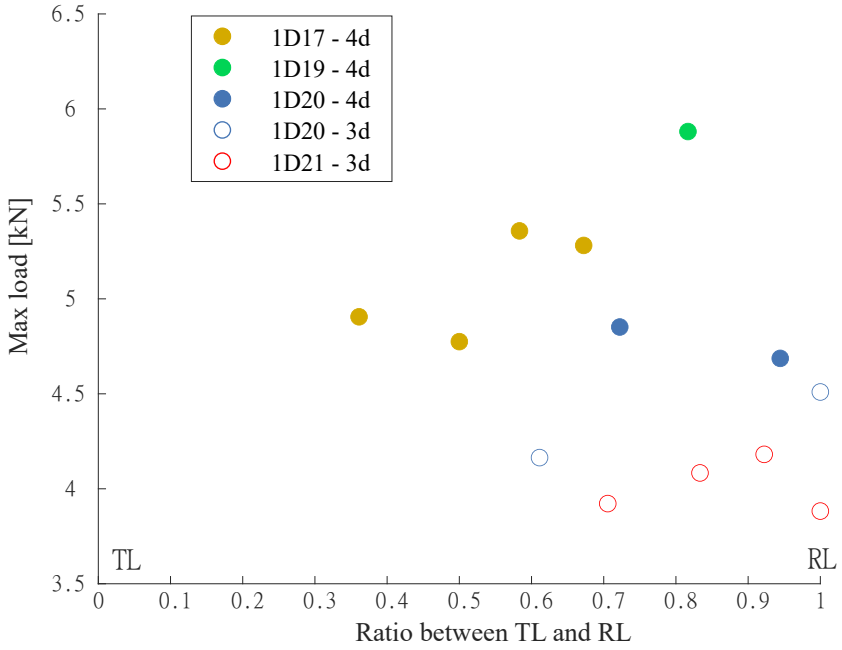

Figure 7.5: The relation between the angle of the crack and the annual growth rings and the maximum load for each beam. 1 is a fracture in pure RL and 0 is a fracture in pure TL.

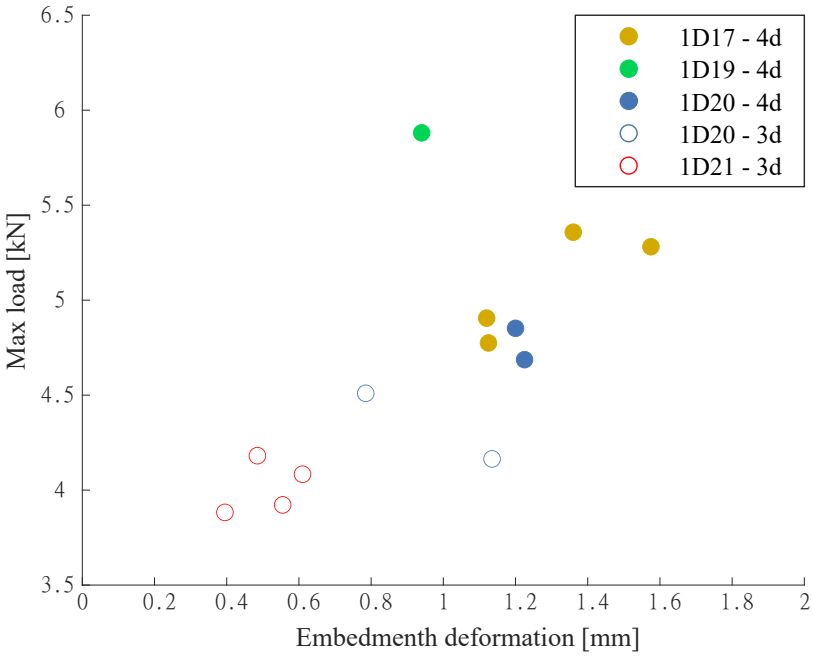

Figure 7.6: The relation between the embedment deformation and the maximum load for each beam.

7.2.1 Observations of experimental dowel test results

Looking at figure 7.4, test 1D19 showed a higher capacity than the other test, which may be due to the high density of the specimen. Looking at figure 7.6, the embedment deformation was not as big in relation to the maximum load for the 1D19 series, compared to the rest. Since only one beam was tested from series 1D19 it is not possible to make any conclusions about the behavior for this series.

In figure 7.4, there could be a trend of the maximum load increasing as the density increases for the beams with an edge distance of $4d$. This could be due to the fact that embedment strength is partly based on density as seen in section 4.1. A higher density gives a higher embedment strength, leading to a decreased risk for deformation in the hole where the dowel was placed. When observing the edge distance of $3d$, in figure 7.4, the maximum load decreased with the increased density, which may be due to knots but also due to the splitting capacity not being density dependent (according to formula 7.1).

By studying the relation between the angle of the annual growth ring and the crack and the maximum load, shown in figure 7.5, no clear trends are seen. The capacity of the beam is not only dependent of in which direction the growth rings are oriented. The capacity could also be affected by present knots. The TL-RL relations between the crack and the annual growth rings are shown for all series in figure 7.15 and 7.16.

While the cubes used for testing the fracture energy were as close to clear wood as possible, the beams had apparent knots which could have affected the capacity. Looking at table 7.6, beam 1D21D has a TL-RL ratio of 1.0 (pure RL loading) which suggests a higher splitting capacity since $G_{c,RL} > G_{c.TL}$. However, the measured maximum load was not higher for 1D21D than the other beams in the 1D21-series, which maybe was due to the knots showed in figure 7.13 and 7.14.

Observing figure 7.11, 7.12 and 7.14, the fracture plane of 1D20B, 1D20D and 1D21D is passing straight through a knot which might have influenced the capacity. The location of where the angle was measured, at the beam-ends, might not be preferable since the angle of the fracture plane could vary over the length of the beam. The results in figure 7.5 could therefore be deceptive.

By studying the beams after the test was performed, a deformation of the pre-drilled hole could be seen, especially in the beams with an edge distance of $4d$. The micro cracking around the pre-drilled hole, as seen in figure 7.17, is a possible explanation to the plateau (at approximately 3.5 - 4.0 kN) appearing in figure 7.2. This conclusion is suggested since the micro cracks visually started to appear at the same time as the plateau appeared during the experimental testing.

7.2.2 Comparing calculated and experimental results

Figure 7.7 shows the calculated splitting capacity and experimental results for the beams. The average fracture energies, $G_{c,RL}$ and $G_{c,TL}$, and the shear modulus, G_{TL} and G_{RL}, from table 7.1 were used. The beams' experimental capacity was predicted to be within the interval, F_{RL} and F_{TL}, shown in the figure. F_{RL} was calculated using only G_{RL}, whereas F_{TL} was calculated by only using G_{TL}. The intervals were created by inserting both $G_{c,RL,min}$ and $G_{c,RL,max}$ from table 6.7 into equation 7.1 to obtain F_{RL} and F_{TL}. The F_{EC} curve illustrates equation 4.16, which is based on softwoods. It can be observed in the figure that the expected and experimental results do not align.

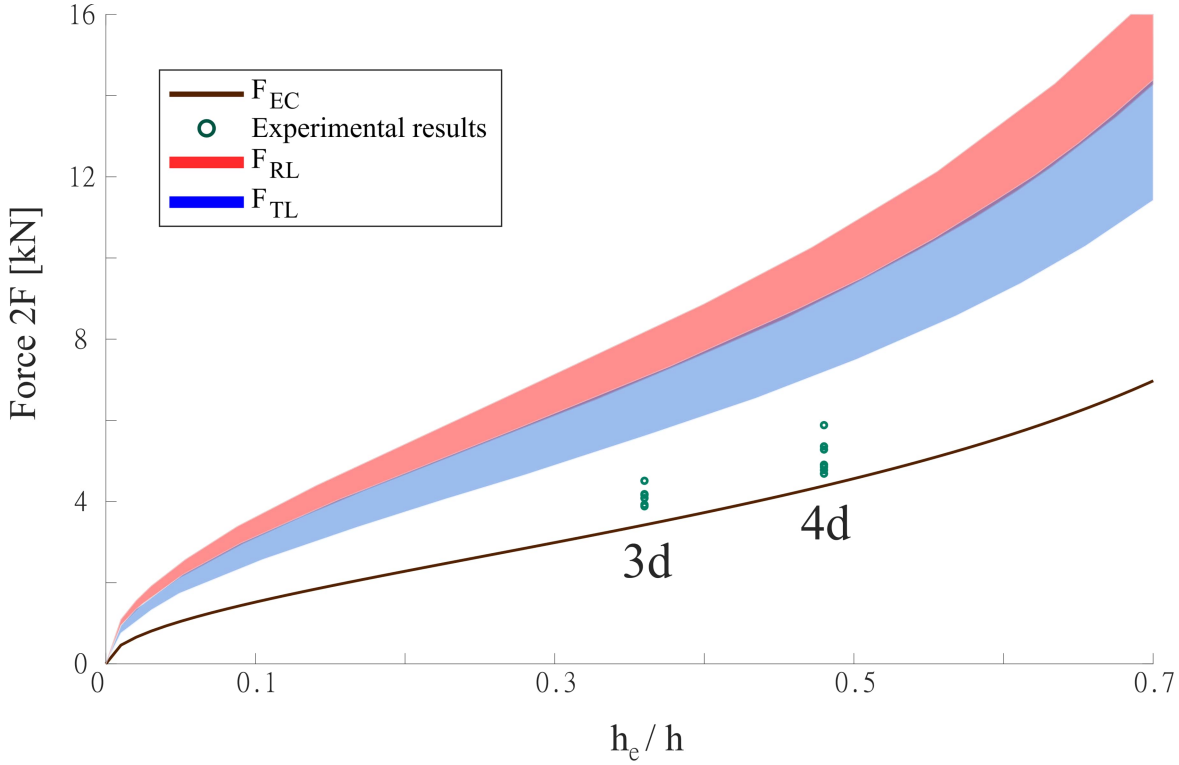

Figure 7.7: Experimental results (dots) for different dowel edge distances, compared to calculated results (the span) using using $G_{c,RL}$ (red), $G_{c,TL}$ (blue). The splitting capacity of softwood (brown), according to Eurocode 5, is also shown.

7.2.3 Observations - Comparing calculated and experimental results

Comparing the calculated capacity with the experimental results, it is seen that the strength of the beam is highly overestimated. The low capacity of the beam could be explained by the mixed failure behaviour, being a combination between a pure splitting and an embedment failure. The mixed mode is, according to [20], directly related to the formation of small cracks in the wood where the dowel is applying its force, in this case at the top of the pre-drilled hole. It could also be related to the deformation of the wood around the connection. This correlation is seen clearly when observing the force-deformation curve for the beams. Beam 1D21D shows that the most brittle behavior of the beams could be related to the deformation of the hole being smaller, as shown in table 7.6. When observing the beams and the small cracks around the pre-drilled hole, it is clearly seen that this beam (1D21D) also has the lowest amount of cracks. Contrary, the beams from the 1D17 series have larger deformations and high amounts of micro cracks, when observing figure 7.2. This may be correlated to the 1D17 series having a larger maximum capacity.

Even though the calculated capacity is overestimated, the experimental maximum loads increases with an increased relative edge distance, h_e/h, as seen in figure 7.7. A reason for the difference between the experimental and calculated capacity could be that clear wood was used during the fracture energy tests. When testing the splitting capacity of the beams, knots and other defect were present, see figure 7.11. The extent to which the knots affect the capacity of the wood is unknown, but it could be assumed that the capacity could both be increased or decreased in some extent.

7.2.4 Photos of series 1D17-21 from the experimental testing

Here the series are presented after after the dowel tests. The load direction, the cracking along the beam and the cracks at the beam ends are presented.

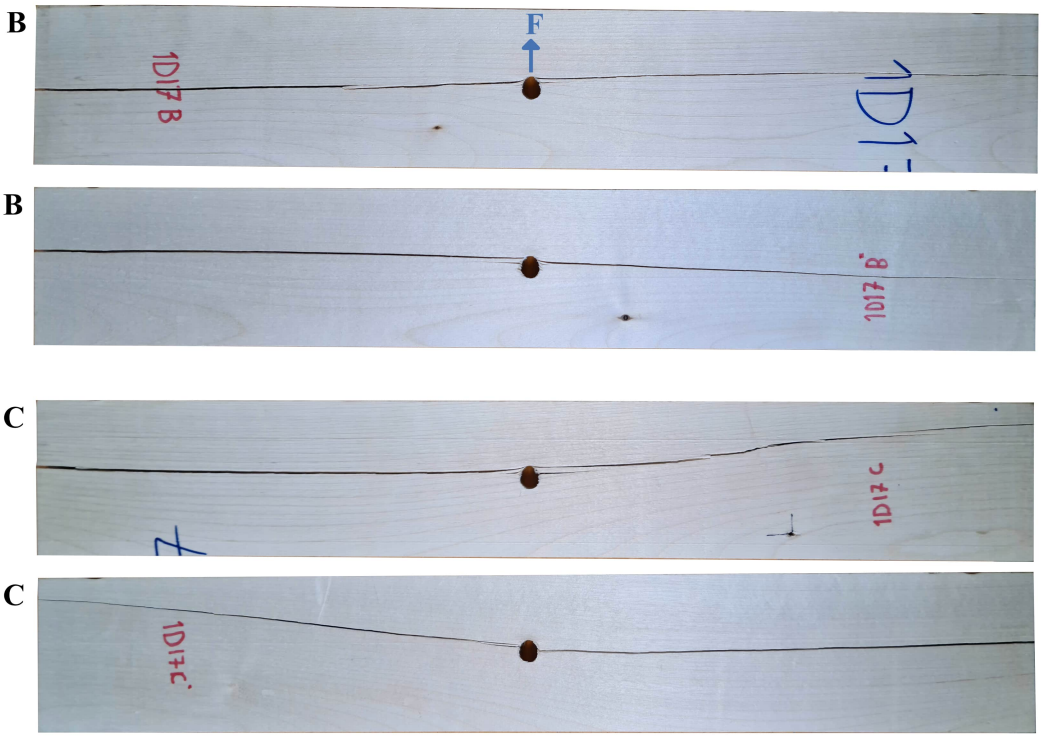

Figure 7.8: Beam 1D17B and 1D17C after the dowel tests.

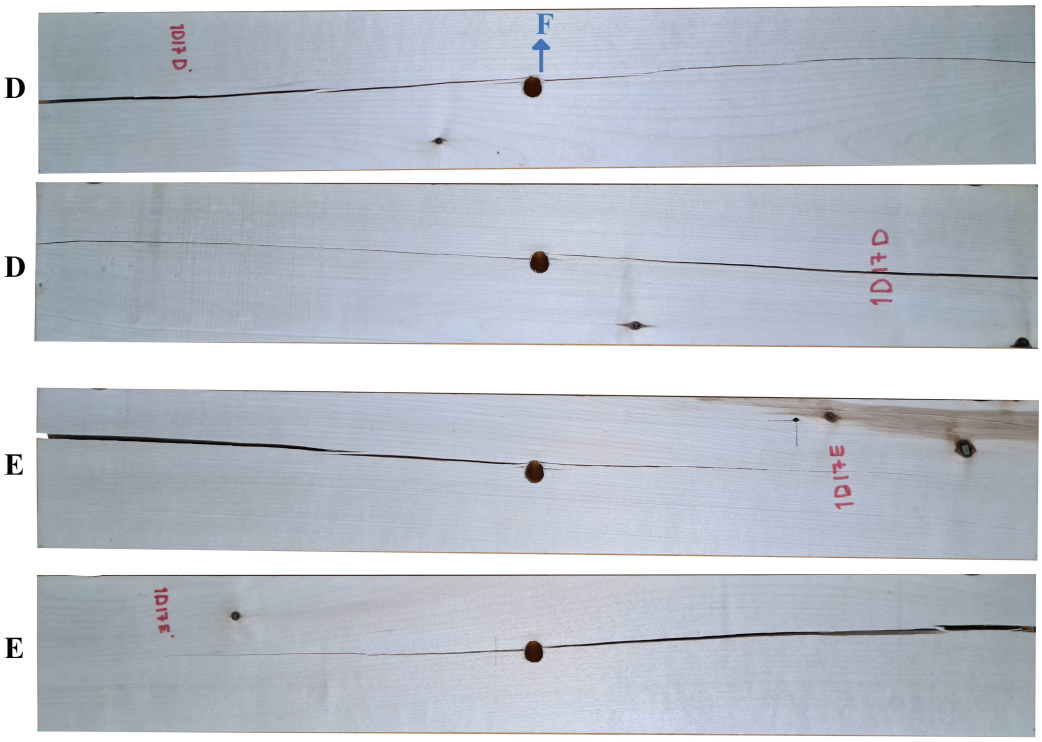

Figure 7.9: Beam 1D17D and 1D17E after the dowel tests.

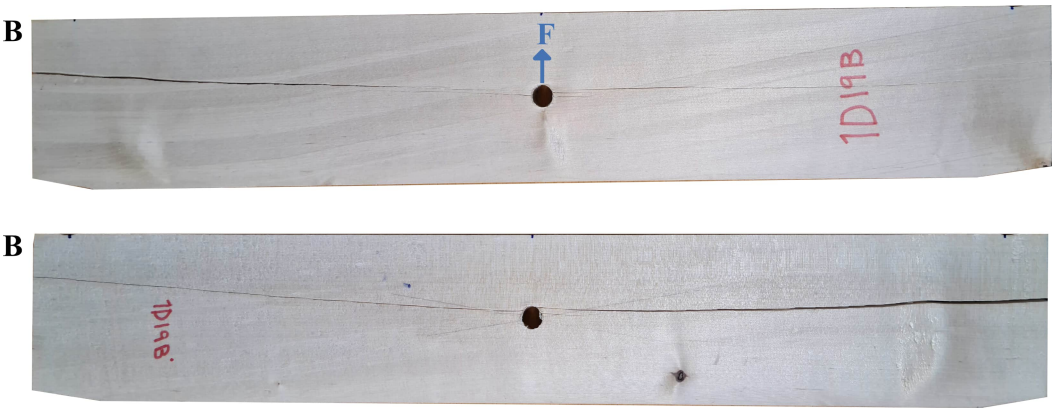

Figure 7.10: Beam 1D19D after the dowel tests.

Figure 7.11: Beam 1D20B and 1D20C after the dowel tests.

Figure 7.12: Beam 1D20D and 1D20E after the dowel tests.

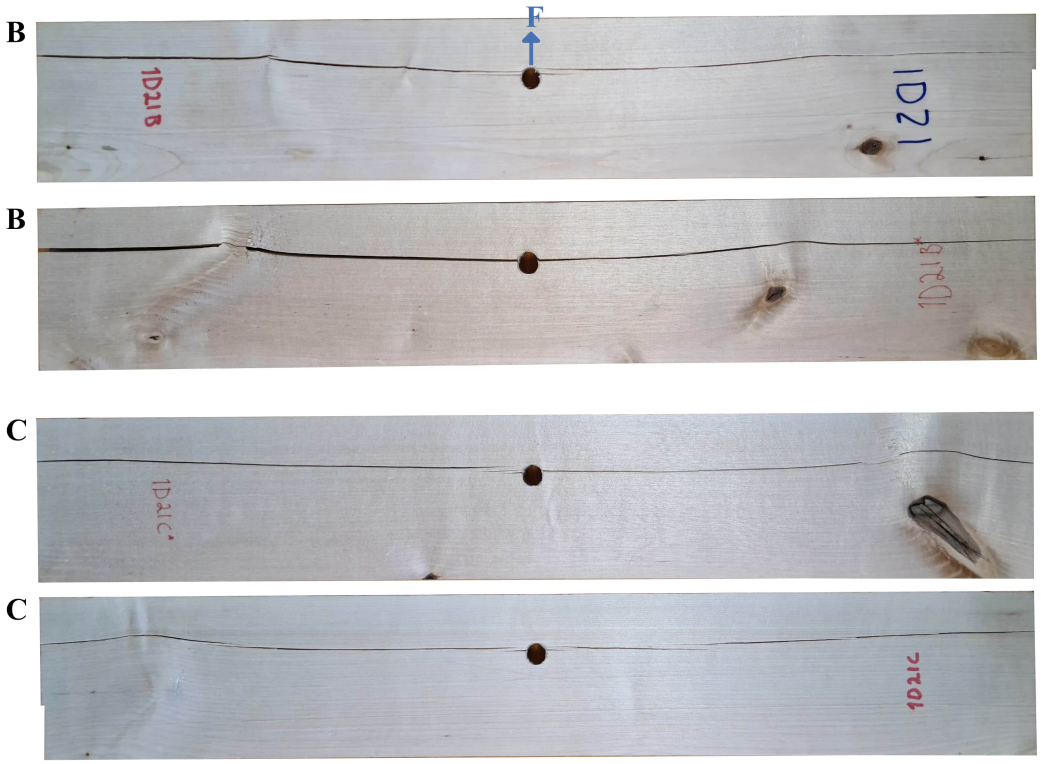

Figure 7.13: Beam 1D21B and 1D21C after the dowel tests.

Figure 7.14: Beam 1D21D and 1D21E after the dowel tests.

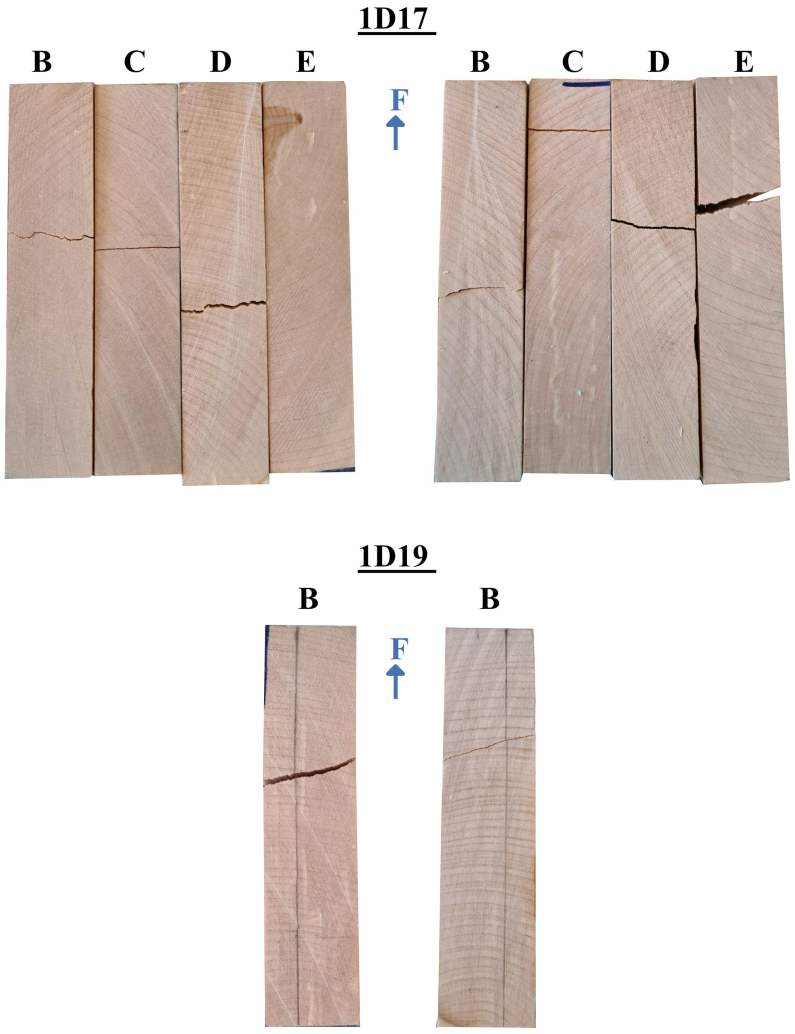

Figure 7.15: The beam ends for series 1D17 and 1D19.

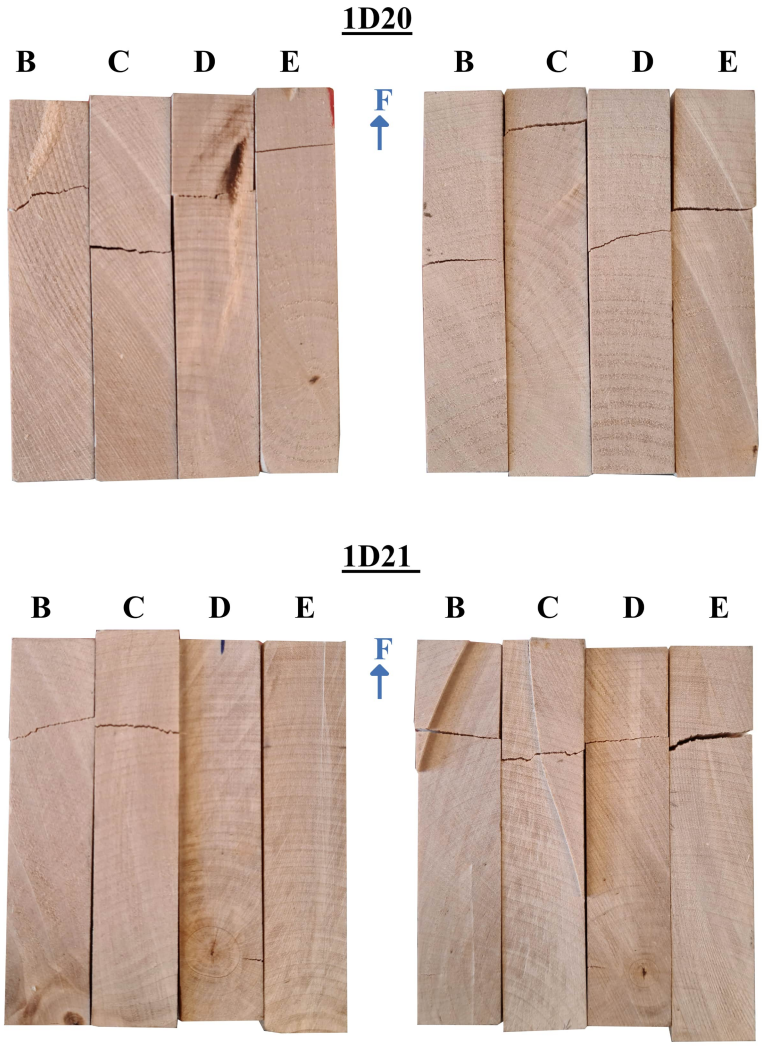

Figure 7.16: The beam ends for series 1D20 and 1D21.

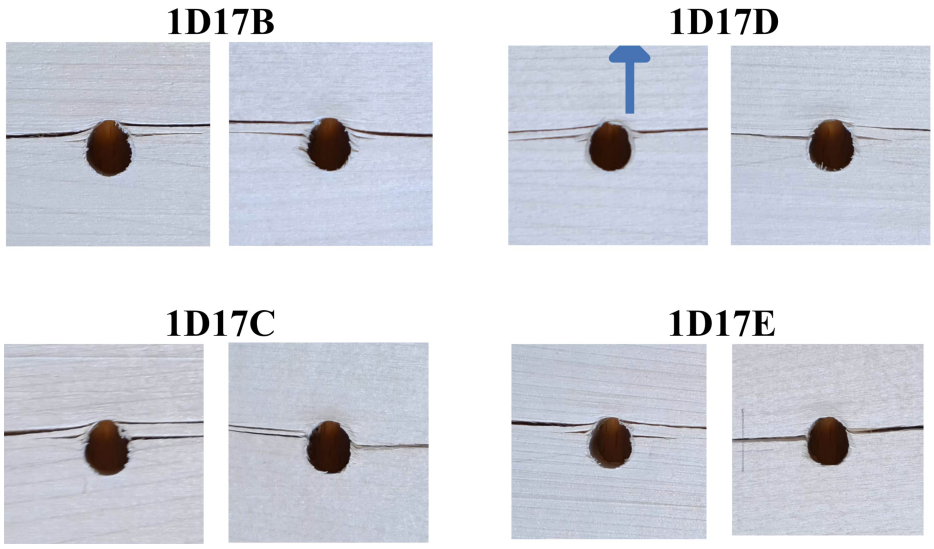

Figure 7.17: Dowel-hole deformations for series 1D17.

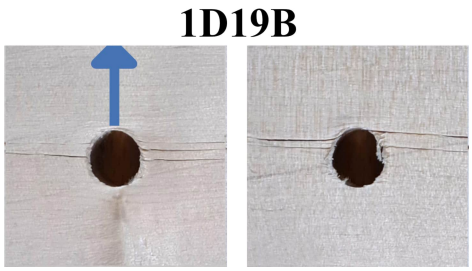

Figure 7.18: Dowel-hole deformations for series 1D19.

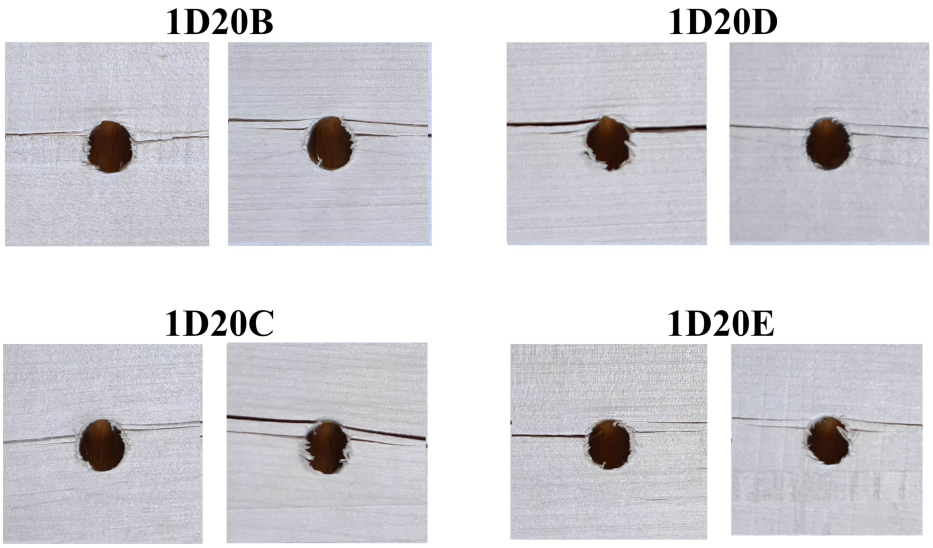

Figure 7.19: Dowel-hole deformations for series 1D20.

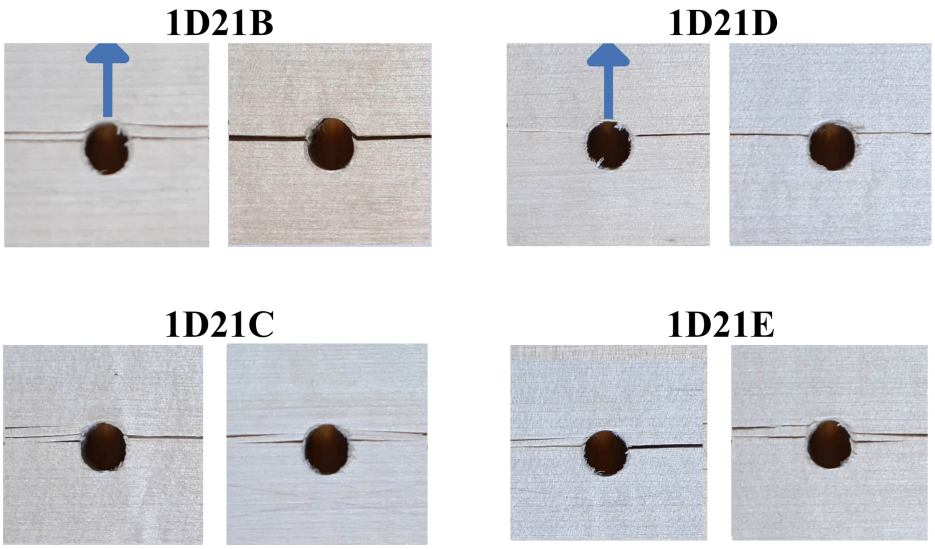

Figure 7.20: Dowel-hole deformations for series 1D21.

8 Discussion and conclusions

8.1 Summary of results

Experimental work was performed to obtain the fracture energy in Swedish birch, using the Nordtest method. The fracture energy was determined in two different crack plane orientations, radial-longitudinal (RL) and tangential-longitudinal (TL).

- The mean value of the fracture energy obtained from the stable responses was 467 J/m^2 in the RL direction and 435 J/m^2 in the TL direction.
- When the experiments for determining the fracture energy in birch were conducted, two different shapes of fracture areas were used, rectangular and triangular. When using a rectangular shaped notch, 8/8 specimens showed an unstable response when tested in the RL direction. Contrary, only 1/8 in the TL direction showed an unstable response. For the specimens with a triangular shaped notch, all of the specimens (8/8 + 8/8) showed a stable response for the RL and TL directions.
- The maximum load was 55% lower for the specimens with a triangular shaped fracture area than for the ones with a rectangular ones. Only the stable responses were compared in this regard.
- The average value of the density of the specimens (the ones tested for fracture energy) was measured to 648 kg/m^3 with a coefficient variation of 5.3 %.

The experimentally evaluated fracture energy was used to calculate the splitting capacity of dowel-typ joints. A test setup was produced consisting of a dowel and a beam cut from the same planks used in the earlier fracture energy experiments.

- Moving the dowel placement from $4d$ to $3d$ yielded a lower maximum load. The material with an edge distance of $4d$ showed a higher maximum capacity compared to the beams with an edge distance of $3d$.
- The beams with a higher load capacity generally had a larger hole deformation.
- The beams with an edge distance of $3d$ reached their maximum capacity around the same time the beams with an edge distance of $4d$ started to show increased embedment deformations.
- The experimental results for maximum loading capacity were lower than the calculated splitting capacity.
- The mean density of the beams tested with dowel-type joints was measured to be 609 kg/m^3, with a coefficient of variation of 3.7%.

8.2 Discussion

The birch material used in this study was provided from RISE, Research Institute of Sweden. The material in this study is a subset of the material used for a larger experimental study regarding density, bending strength and the modulus of elasticity [6]. The measured mean value for the density in those tests was 620 kg/m^3, this is low compared to the measured mean density in this study where the four series, 1D17-21, had a mean density of 609-682 kg/m^3. All of the series are still within the 95^{th} percentile, based on the density in the project by RISE. In their study, the density is measured on clear wood and therefore only the density of the cubes, not the beams, in this study can be compared. In our study, the density of the beams is lower than the test cubes', probably due to defects. Another reason for beams' lower density could be due to uncertainties when measuring their volume, since they could be slightly twisted or bent.

The fracture energy obtained in this study, 435 J/m^2 in the TL direction, could be compared to the results that Forsman [12] and Plönning and Lai [8] found. In Forsman's thesis, the material used was Swedish birch, with a mean density of 647 kg/m^3 and a moisture content of 13.6 %. The mean fracture energy were measured to 460 J/m^2. In the study that Plönning and Lai conducted, the same material was used. However, the mean density was instead 669 kg/m^3 and the moisture content was 11%. The mean fracture energy for the stable tests was 449 J/m^2. In our study the specimens had a mean density of 648 kg/m^3 and a moisture content of 12%. In summary, the measured fracture energy obtained in the TL direction, in this study, is similar to the earlier studies.

The results in chapter 6 suggest that wood generally has a higher fracture energy in the RL direction, rather than the TL direction. This has also been shown in earlier studies but for other species, e.g in a study made by Reiterer [21] where the species alder, ash, and oak where tested. The number of tests in our study is not enough to make a conclusion regarding the fracture energy. But, it could be seen as an indication that the birch has a higher fracture energy in the RL direction, compared to the TL direction. The difference in RL and TL direction could be explained by the higher volume of rays being present in the radial direction which, in turn,acts as a reinforcement. The TL direction may not be supported by as many rays, making it the weaker direction.

When implementing the fracture energy in dowel-type joint calculations, described in chapter 7, it is difficult to know whether the RL or TL fracture energy should be used. Here, only small tendencies could be seen that a beam with a higher TL-RL ratio showed a higher maximum load before failing, but not enough to make a conclusion.

When comparing the suggested formula for hardwood's splitting capacity to the experimental results, the formula suggested that the splitting capacity was higher than the acquired experimental results. This may be due to knots weakening the beams. The difference between calculated and experimental results can also be due to combinations of embedment failure, splitting and micro cracks weakening the beam. Knots were recorded on most beams. The shear modulus used for calculations was based upon other literature, not experimental data from this project. Therefore, it could have been overestimated, resulting in inaccurate results.

It was concluded in the study by Forsman [12] that the suggested formula from Eurocode 5 overestimated the joint capacities, when comparing the calculated and experimental results for untreated birch. This could also be seen in our study study, see figure 7.7, where all of the experimental tests showed a lower capacity than the calculated capacity.

It appears that the modifications made to the Nordtest method in our study increase the probability of achieving a stable fracture. The higher amount of elastic energy stored in the material, the higher probability of receiving an unstable response. When looking at the studies done by Plönning and Lai [8], a stable response was only obtained in 33% of the tests for birch with a triangular notch, tested in the TL direction. The modification made in our study, changing the height of the rectangular notch from $0.5a$ to $0.6a$, seems to have made a difference since all of the specimens showed a stable response in the TL. Additionally, all but one showed stable responses in the RL direction. Also, when looking at the micro structure of the wood, hardwoods have shorter longitudinal cells, compared to softwoods. The short fibres lead to the energy dissipating processes, like fiber bridging, being less effective [21]. This could be a explanation as to why the Nordtest method typically gives stable results for softwoods, compared to the many unstable responses from the tests on the hardwoods.

The high difference (55%) in maximum load capacity, when using a rectangular and a triangular shaped notch, was anticipated. Aligning with the study by Lai and Plönning, both experiments and simulations demonstrated a significant increase in maximum load capacity when using a rectangular notch.

9 Further work and studies

It would be of interest to investigate if the shape of the fracture area influence the obtained fracture energy. This could be done by investigating a material that show a stable behaviour independent of the shape.

The embedment strength for the material should be tested and evaluated.

The shear modulus used in the calculations is an estimated value, this should be looked into more. The shear modulus is vital for estimating the fracture loading and should therefore be better known.

The tensile strength perpendicular to the grain could be useful when using non-linear modeling on e.g dowel-type joints. The tensile strength perpendicular to the grain could be evaluated by applying tensile forces on smaller test specimen, compared to the beams in our study. This has been done in a study by Forsman [12] where a small cube, of similar dimension to the one in our study (in the Nordtest method), was subjected to pure tensile loading. This was done by gluing the cube to two parallel surfaces in an MTS machine and applying a tensile force. Measuring the maximum force and dividing it by the area would then yield the tensile strength perpendicular to the grain.

Bibliography

[1] Swedish Wood. *Wood facts*. Available from: http://www.swedishwood.com/wood-facts/. [Cited: 2024-01-22].

[2] Träguiden. *Skog och skogssköttsel*. Available from: https://www.traguiden.se/om-tra/materialet-tra/skogsbruk/skogsbruk/skogsskotsel/. [Cited: 2024-01-25].

[3] Skogskunskap. *Björk*. Avilable from: https://www.skogskunskap.se/skota-lovskog/om-lov/vara-lovtrad/bjork-betula-spp/. [Cited: 2024-02-20].

[4] Klimatanpassning. *Skogsbruk*. Available from: https://www.klimatanpassning.se/hur-samhallet-paverkas/areella-naringar/skogsbruk-1.21503. [Cited: 2024-01-25].

[5] "Varför sågas så lite björk i Sverige? : Why isn't more birch wood being sawn in Sweden?" Växjö Univeritet. PhD thesis. URL: https://urn.kb.se/resolve?urn=urn:nbn:se:vxu:diva-6364.

[6] U. Lemke, M. Johansson, R. Ziethén and Andreas Briggert. "New Criteria For Visual Strength Grading of Sawn Timber From Birch Grown In Sweden". In: *World Conference on Timber Engineering (WCTE 2023) : Timber for a Livable Future*. World Conference on Timber Engineering (WCTE), 2023, pp. 740–749. ISBN: 9781713873273. DOI: 10.52202/069179-0102.

[7] Per Johan Gustafsson. *Nordtest; Wood: Fracture Energy in Tension Perpendicular to the Grain*. English. Vol. NT Build 422. TVSM-7000 TVSM-7074. Nordtest, Nordic Innovation, 1994.

[8] Lai, Gary and Plönning, Samuel. *Fracture characteristics of acetylated birch - Experimental and numerical studies*. Master's dissertation, Report TVSM-5000, Division of Structural Mechanics, Lund University. 2019.

[9] Dinwoodie J.M. *Timber: Its Nature and Behaviour. [Elektronisk resurs]*. CRC Press, 2002. ISBN: 9780415515153.

[10] *Dimensionering av träkonstruktioner. Del 1*. Skogsindustrierna, Svenskt trä, 2019. ISBN: 9789198521474.

[11] Lars Wadsöö. *Construction Materials Science*. Division of Building Materials.

[12] Forsman, Karin. *Fracture behaviour of acetylated wood : Material characterisation and dowel-type connections*. Licentiate Thesis, Report TVSM-3081, Division of Structural Mechanics, Lund Univeristy. 2020.

[13] Rubin Shmulsky and P David Jones. "Forest products and wood science: an introduction". In: (2019).

[14] Aicher, Simon and Gustafsson, Per Johan and Haller, Peer and Petersson, Hans. *Fracture Mechanics Models for Strength Analysis of Timber Beams with a Hole or a Notch : A Report of RILEM TC-133*. Report TVSM-7134, Division of Structural Mechanics, LTH.

[15] Henrik Danielsson. *Perpendicular to grain fracture analysis of wooden structural elements : models and applications.* Report TVSM: 1024. Division of Structural Mechanics, Department of Construction Sciences, Lund University, 2013. ISBN: 9789174734751.

[16] *Dimensionering av träkonstruktioner del 2.* Skogsindustrierna, Svenskt Trä, 2019. ISBN: 9789198521481.

[17] TACM Van der Put and AJM Leijten. "Evaluation of perpendicular to grain failure of beams caused by concentrated loads of joints". In: *Proceedings of CIB-W18/paper, paper 33-7-7* (2000), pp. 33–7.

[18] Swedish Standards Institute. *SS-EN 13183-1/AC:2004. Moisture content of a piece of sawn timber –Part 1: Determination by oven dry method.* 2004.

[19] Swedish Standards Institute. *SS-EN 408:2010+A1:2012. Träkonstruktioner – Konstruktionsvirke och limträ – Bestämning av vissa fysikaliska och mekaniska egenskaper.* 2012.

[20] José Luis Gómez-Royuela, Almudena Majano-Majano, Antonio José Lara-Bocanegra, José Xavier and Marcelo F. S. F. de Moura. "Experimental and Numerical Research on the Splitting Capacity of European Beech Beams Loaded Perpendicular to the Grain by Connections: Influence of Different Geometrical Parameters". In: *Applied Sciences* 14.2 (2024). ISSN: 2076-3417. DOI: 10.3390/app14020900. URL: https://www.mdpi.com/2076-3417/14/2/900.

[21] A. Reiterer, G. Sinn and S.E. Stanzl-Tschegg. "Fracture characteristics of different wood species under mode I loading perpendicular to the grain". In: *Materials Science and Engineering: A* 332.1 (2002), pp. 29–36. ISSN: 0921-5093. DOI: https://doi.org/10.1016/S0921-5093(01)01721-X.

Appendix A

Dimensions and weights

A.1 Cubes

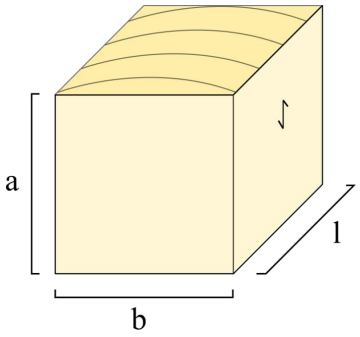

Figure A.1: Figure showing the definitions of the lengths presented in table A.1 and A.2.

Table A.1: Table of measured weight and dimensions for test specimens that were tested for RH.

Specimen ID	Weight [g]	l [mm]	b [mm]	a [mm]	Volume [mm^3]
1D17A5	5.325	20.30	20.20	20.06	8226.82
1D17A10	5.261	20.31	20.24	19.98	8211.24
1D19A5	5.556	20.13	20.25	19.99	8148.55
1D19A10	5.591	20.14	20.25	19.92	8121.05
1D20A5	5.015	20.10	20.08	20.41	8235.57
1D20A10	5.031	20.13	20.14	20.55	8332.36
1D21A5	5.45	20.11	20.14	19.91	8062.84
1D21A10	5.026	20.13	20.09	19.90	8044.77

Table A.2: Table of measured weight and dimensions for test specimens that were tested for fracture energy.

Specimen ID	Weight [g]	l [mm]	b [mm]	a [mm]	Volume [mm^3]	Fracture area [mm^2]
1D17A1	5.297	20.30	20.21	20.00	8205.26	88.44
1D17A2	5.211	20.26	20.21	19.88	8140.96	77.83
1D17A3	5.256	20.30	20.21	20.05	8225.77	79.18
1D17A4	5.283	20.30	20.22	19.50	8000.14	87.73
1D17A6	5.327	20.31	20.22	20.01	8212.38	84.80
1D17A8	5.310	20.32	20.25	20.02	8234.80	82.33
1D17A9	5.330	20.32	20.24	20.10	8264.62	81.24
1D17A11	5.222	20.10	20.20	19.82	8044.89	80.61
1D19A1	5.494	20.07	20.24	19.94	8101.97	172.29
1D19A2	5.393	20.04	20.21	19.93	8071.80	164.12
1D19A3	5.489	20.10	20.25	20.00	8139.47	153.54
1D19A4	5.567	20.14	20.26	20.03	8173.98	155.79
1D19A6	5.576	20.12	20.26	19.95	8131.22	150.89
1D19A7	5.630	20.20	20.27	19.93	8155.35	153.11
1D19A8	5.637	20.12	20.25	19.95	8129.22	165.09
1D19A9	5.575	20.14	20.24	19.90	8106.87	167.60
1D20A2	5.066	20.10	20.10	20.42	8249.87	158.52
1D20A3	5.092	20.13	20.14	20.37	8260.42	162.87
1D20A4	5.054	20.12	20.15	20.38	8258.34	165.41
1D20A6	5.008	20.12	20.13	20.30	8222.83	155.57
1D20A7	5.073	20.12	20.13	20.61	8349.42	162.50
1D20A8	4.975	20.10	20.14	20.44	8273.39	164.36
1D20A9	4.936	20.11	20.14	20.48	8295.73	162.08
1D20A11	4.932	19.87	19.96	20.10	7969.63	157.42
1D21A1	5.084	20.10	20.05	19.90	8017.79	85.03
1D21A2	5.309	20.15	20.08	19.97	8077.09	80.82
1D21A3	5.541	20.20	20.10	19.96	8104.15	86.43
1D21A4	5.844	20.18	20.10	19.94	8086.00	85.74
1D21A6	5.116	20.12	20.13	19.87	8045.67	79.24
1D21A7	5.095	20.12	20.09	19.85	8017.57	79.43
1D21A8	5.053	20.15	20.09	19.87	8041.62	78.09
1D21A9	4.997	20.12	20.10	19.80	8006.35	78.14

A.2 Beams

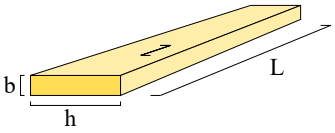

Figure A.2: Figure showing the definitions of the lengths presented in table A.3.

Table A.3: Table of measured weight and dimensions of the beams.

Serial Number	Weigth (g)	L [mm]	b [mm]	h [mm]	Volume [10^3 mm^3]
1D17B	482.10	515	17.7	82.7	753.9
1D17C	476.60	514	17.8	81.4	744.7
1D17D	469.70	514	17.7	82.8	753.3
1D17E	467.60	514	17.8	81.8	748.4
1D19B	470.80	489	18.3	82.3	736.5
1D20B	425.18	497	17.6	82.2	719.0
1D20C	428.05	497	17.9	83.1	739.3
1D20D	436.03	497	17.8	82.9	733.4
1D20E	419.15	497	17.6	82.7	723.4
1D21B	428.88	498	17.8	81.5	722.4
1D21C	448.32	498	17.8	83.0	735.7
1D21D	435.37	498	17.8	81.3	720.7
1D21E	438.74	498	17.8	83.0	735.7

Appendix B

Load-deflection curves

B.1 Cubes

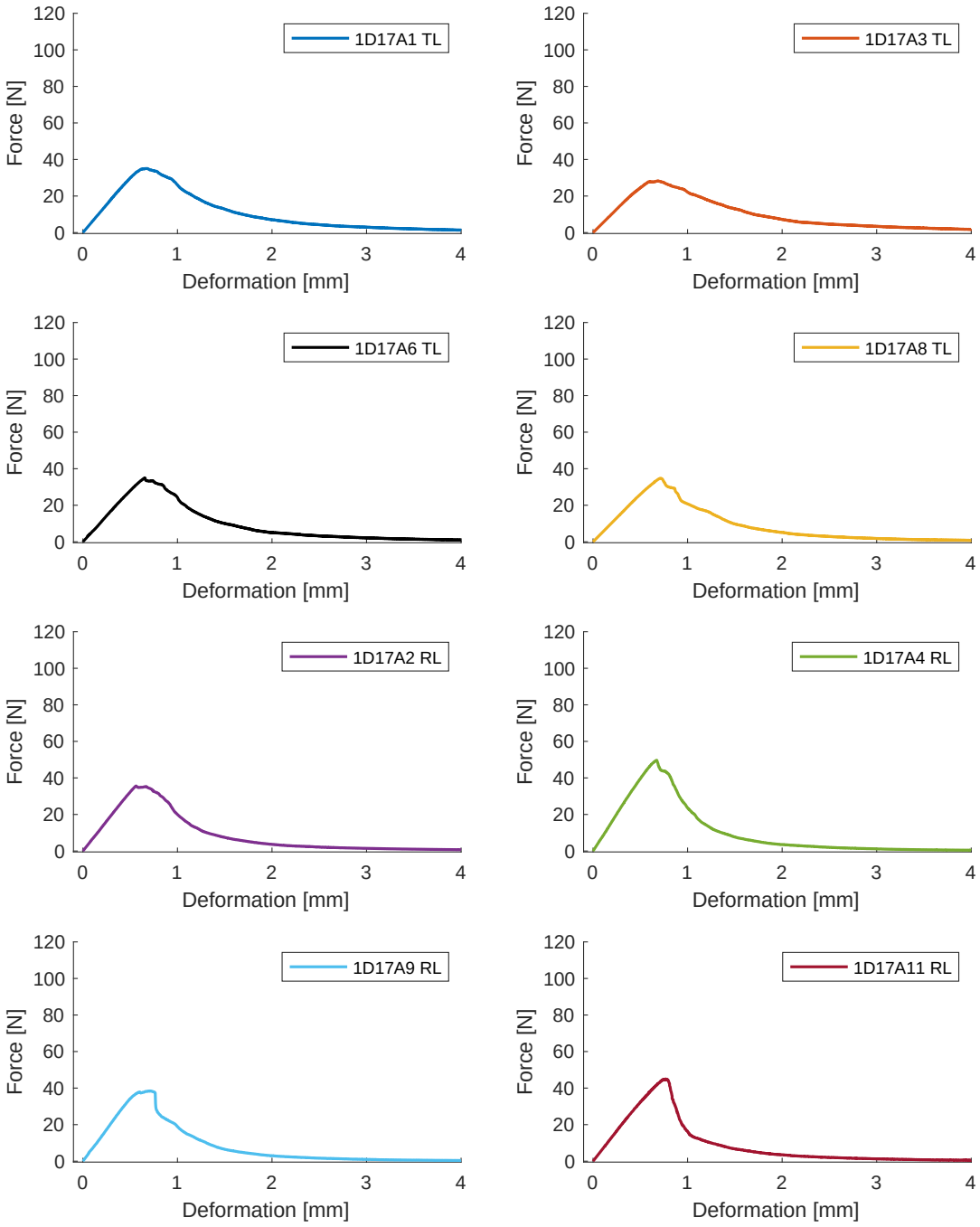

Figure B.1: Load-deflection curves of test specimens from series 1D17A, a series with a triangular fracture area.

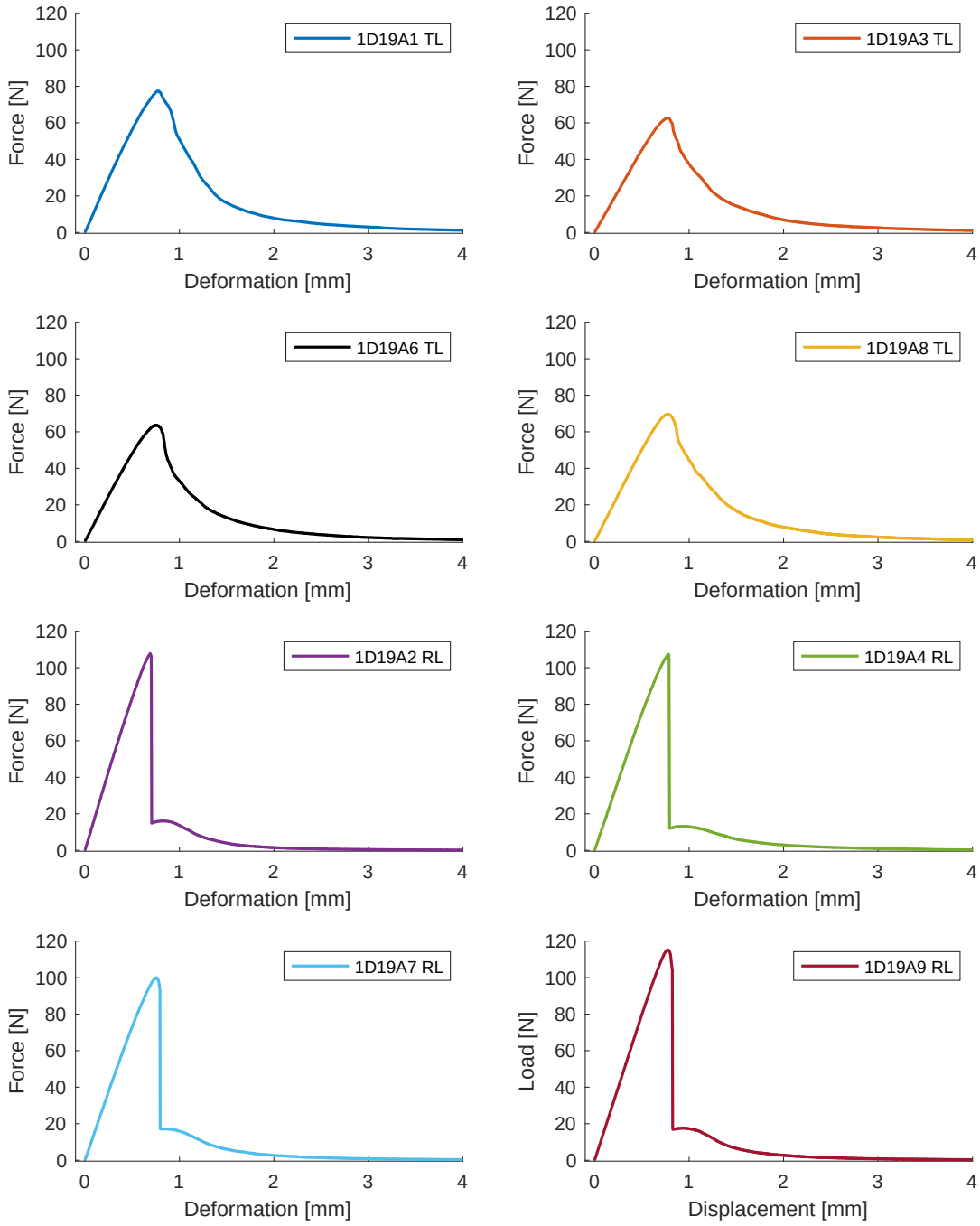

Figure B.2: Load-deflection curves of test specimens from series 1D19A, a series with a rectangular fracture area.

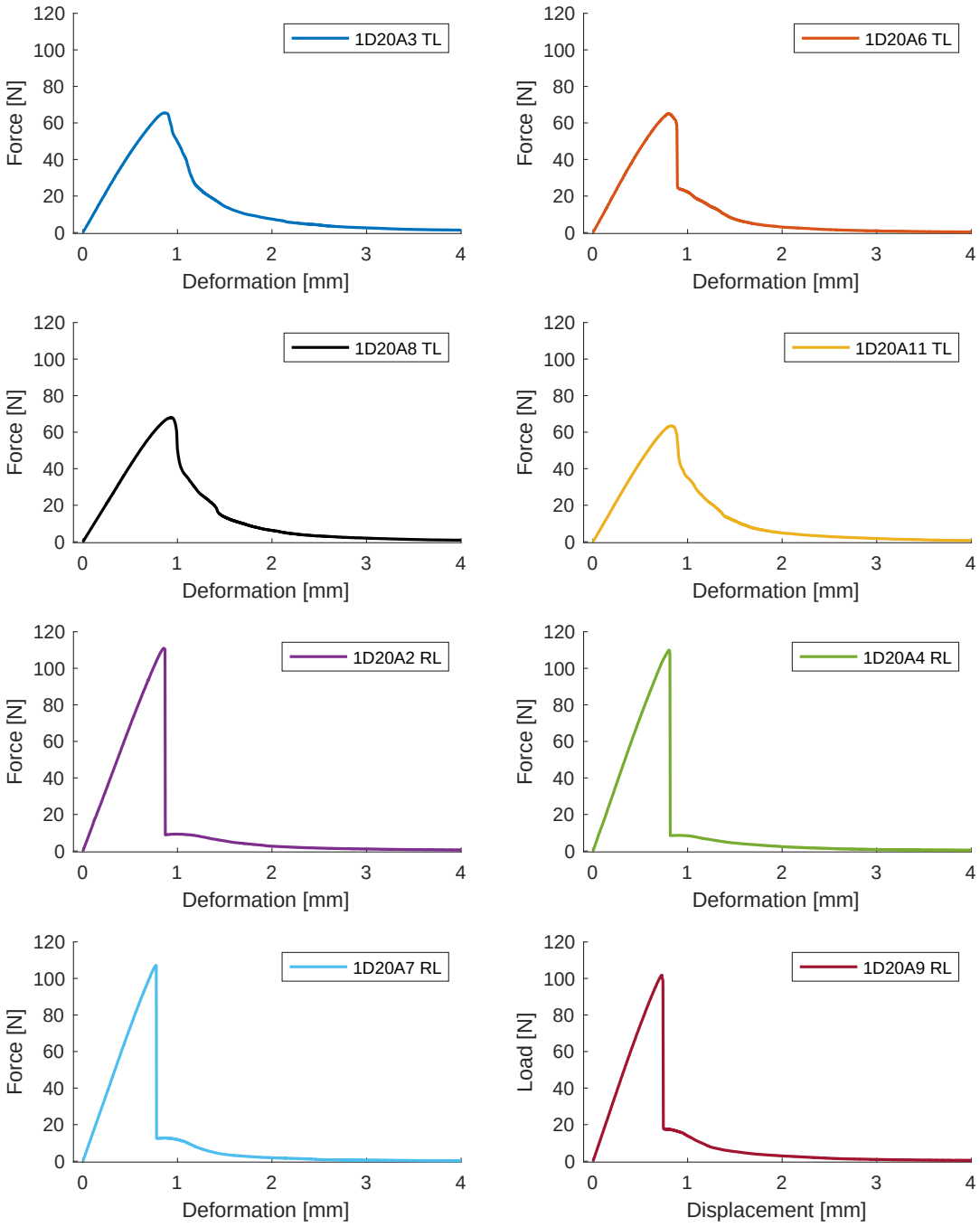

Figure B.3: Load-deflection curves of test specimens from series 1D20A, a series with a rectangular fracture area.

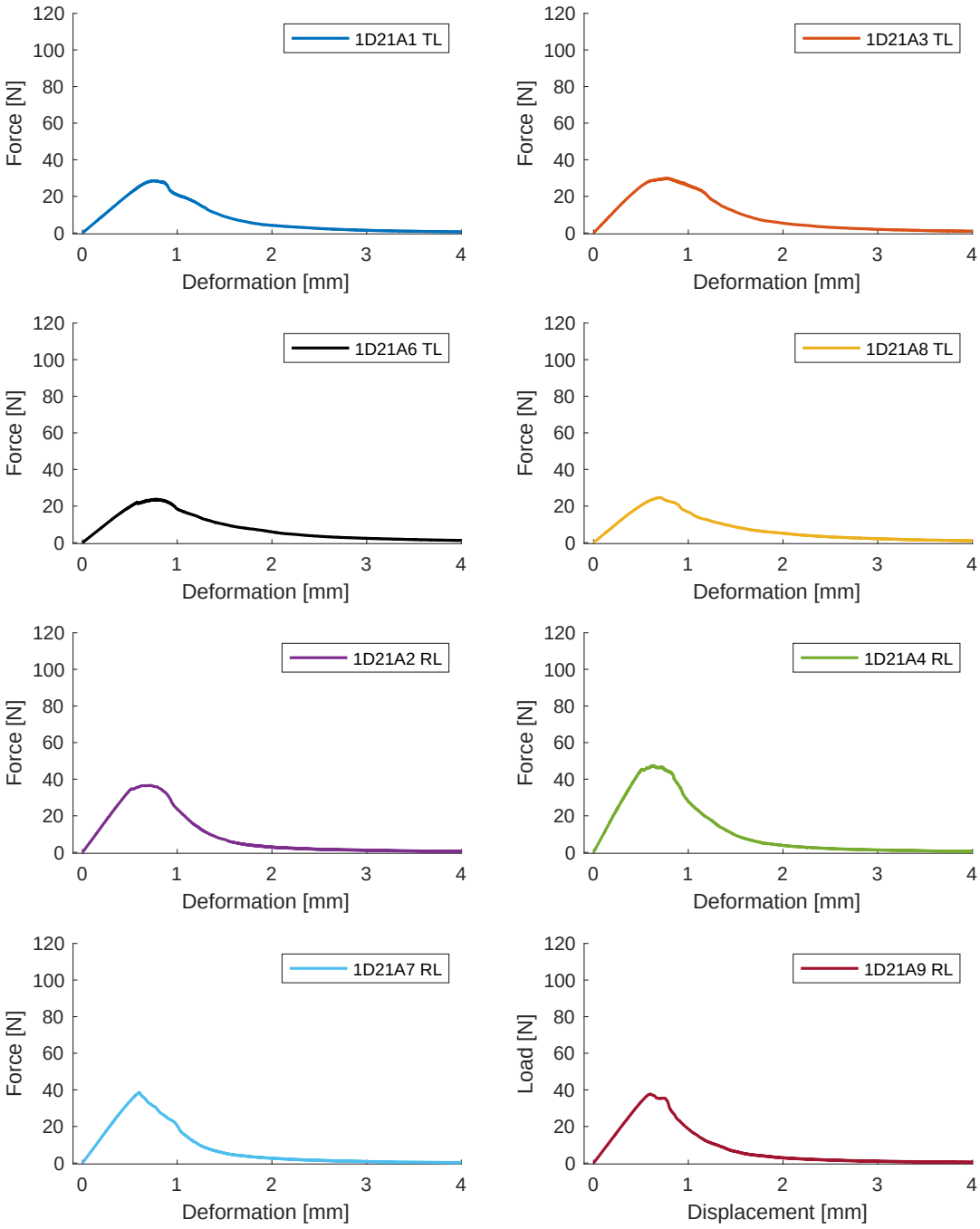

Figure B.4: Load-deflection curves of test specimens from series 1D21A, a series with a triangular fracture area.

B.2 Beams

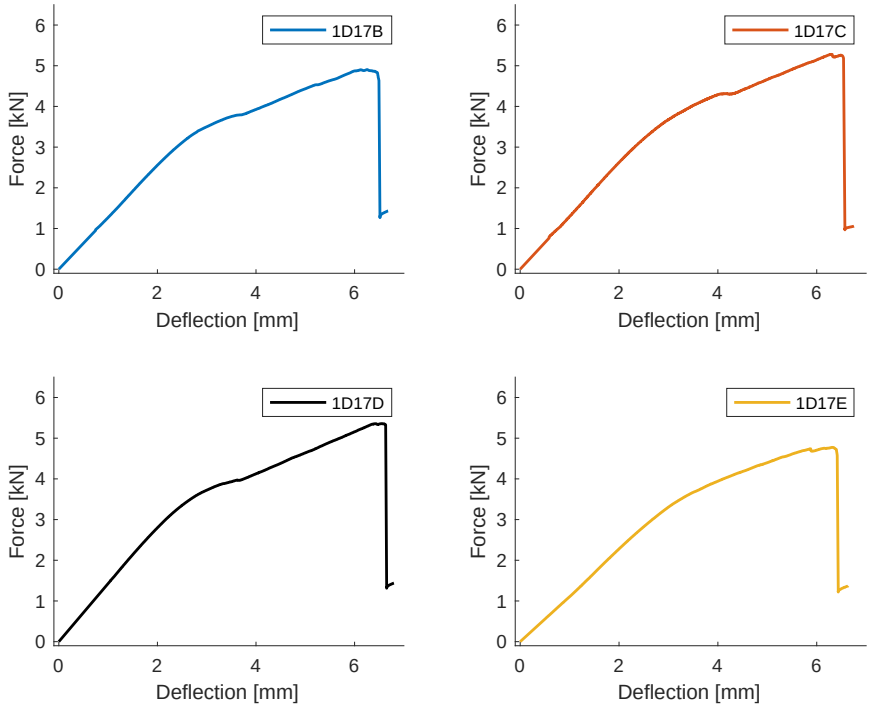

Figure B.5: Load-deflection curves of beams 1D17B-E.

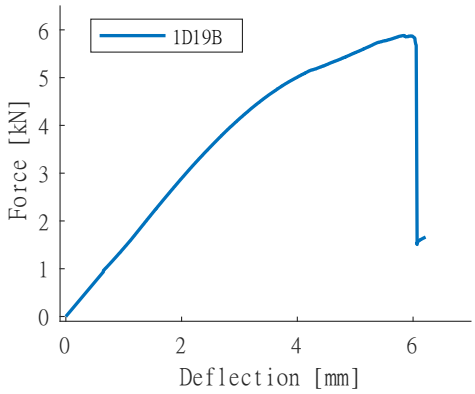

Figure B.6: Load-deflection curve of beam 1D19B.

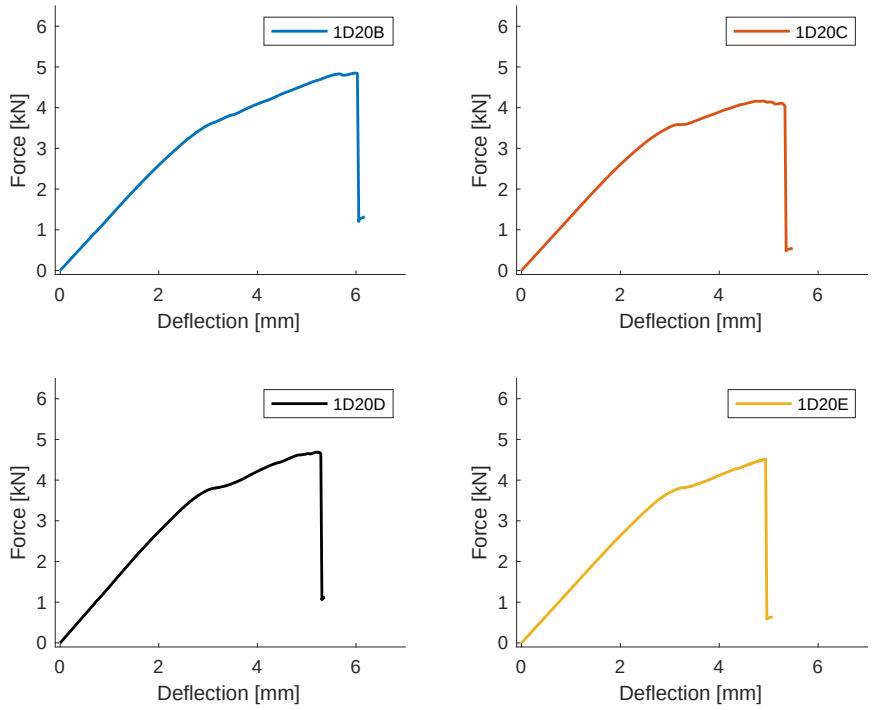

Figure B.7: Load-deflection curves of beams 1D20B-E.

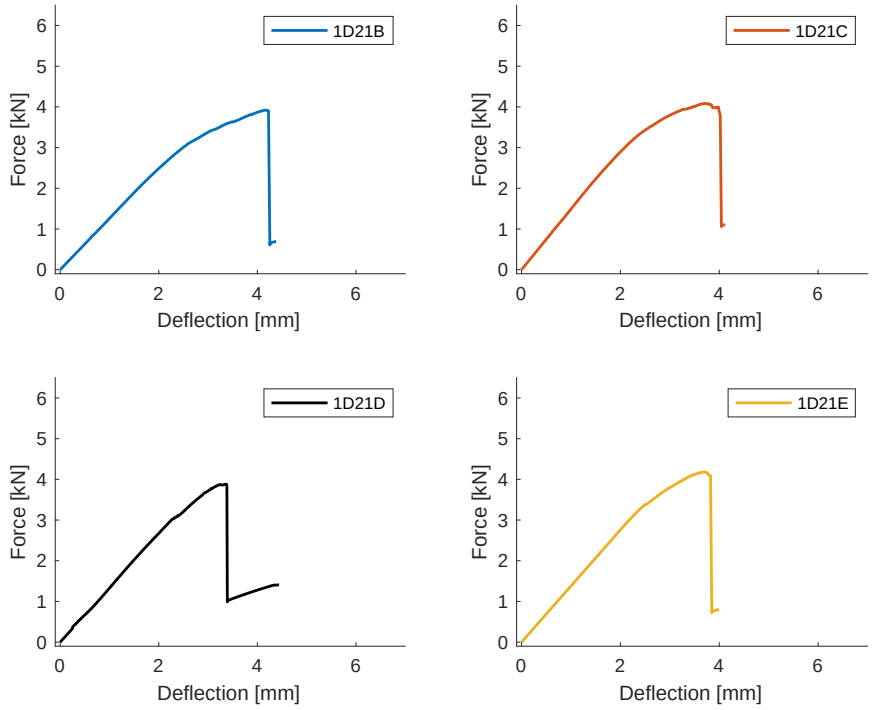

Figure B.8: Load-deflection curves of beams 1D21B-E.